

miRNA-711 Binds and Activates TRPA1 Extracellularly to Evoke Acute and Chronic Pruritus

Highlights

- Intradermal miR-711 evokes itch but not pain via core sequence and TRPA1
- miR-711 is sufficient to activate pruriceptive neurons via TRPA1 in mouse DRG
- The core sequence GGGACCC binds and activates TRPA1 at the extracellular S5-S6 loop
- Skin lymphoma-secreted miR-711 drives itch in a mouse model of chronic itch

Authors

Qingjian Han, Di Liu,
Marino Convertino, ..., Andrea Nackley,
Nikolay V. Dokholyan, Ru-Rong Ji

Correspondence

ru-rong.ji@duke.edu

In Brief

How extracellular miRNA signals is unclear. Han et al. describe that miRNA-711, secreted from inoculated lymphoma cells on the back skin, binds TRPA1 ion channels extracellularly on pruriceptive neurons to drive acute and chronic itch via specific core sequence.

miRNA-711 Binds and Activates TRPA1 Extracellularly to Evoke Acute and Chronic Pruritus

Qingjian Han,^{1,4} Di Liu,^{1,4} Marino Convertino,² Zilong Wang,¹ Changyu Jiang,¹ Yong Ho Kim,¹ Xin Luo,¹ Xin Zhang,¹ Andrea Nackley,¹ Nikolay V. Dokholyan,^{2,5} and Ru-Rong Ji^{1,3,6,*}

¹Center for Translational Pain Medicine, Department of Anesthesiology, Duke University Medical Center, Durham, NC 27710, USA

²Department of Biochemistry and Biophysics, University of North Carolina, Chapel Hill, NC 27599, USA

³Department of Neurobiology, Duke University Medical Center, Durham, NC 27710, USA

⁴These authors contributed equally

⁵Present address: Departments of Pharmacology and Biochemistry and Molecular Biology, Pennsylvania State Medical Center, Hershey, PA 17033, USA

⁶Lead Contact

*Correspondence: ru-rong.ji@duke.edu

<https://doi.org/10.1016/j.neuron.2018.06.039>

SUMMARY

Increasing evidence suggests that extracellular miRNAs may serve as biomarkers of diseases, but the physiological relevance of extracellular miRNA is unclear. We find that intradermal cheek injection of miR-711 induces TRPA1-dependent itch (scratching) without pain (wiping) in naive mice. Extracellular perfusion of miR-711 induces TRPA1 currents in both *Trpa1*-expressing heterologous cells and native sensory neurons through the core sequence GGGACCC. Computer simulations reveal that the core sequence binds several residues at the extracellular S5-S6 loop of TRPA1, which are critical for TRPA1 activation by miR-711 but not allyl isothiocyanate. Intradermal inoculation of human Myla cells induces lymphoma and chronic itch in immune-deficient mice, associated with increased serum levels of miR-711, secreted from cancer cells. Lymphoma-induced chronic itch is suppressed by miR-711 inhibitor and a blocking peptide that disrupts the miR-711/TRPA1 interaction. Our findings demonstrated an unconventional physiological role of extracellular naked miRNAs as itch mediators and ion channel modulators.

INTRODUCTION

MicroRNAs (miRNAs) bind the 3' untranslated regions of mRNAs to regulate gene expression post-transcriptionally (Bartel, 2004). Recent studies suggest that miRNAs may have extracellular roles. Circulating miRNAs are present in various body fluids and serve as biomarkers for diseases (Chen et al., 2008; Lehmann et al., 2012; Qureshi et al., 2016). Analysis of cerebrospinal fluid of Alzheimer's patients revealed an increase of miRNA let-7b (miR-let-7b), which binds toll-like receptor 7 (TLR7) in

cortical neurons to induce neurodegeneration (Lehmann et al., 2012). Following neuronal activation, miR-let-7b is also released by primary sensory neurons of dorsal root ganglion (DRG) (Park et al., 2014). miR-let-7b binds neuronal TLR7 and excites nociceptive neurons, and hind paw injection of let-7b is sufficient to trigger spontaneous pain. This neuronal activation requires TLR7 and specific coupling of TLR7 with transient receptor potential ion channels A1 (TRPA1) (Park et al., 2014). However, it is still unknown whether miRNA can elicit biological responses via TLR-independent mechanisms.

Recent progress has advanced our understanding of molecular and cellular mechanisms of itch (Ji, 2018; LaMotte et al., 2014; Meixiong and Dong, 2017), including but not limited to the receptors of itch (Alemi et al., 2013; Liu et al., 2009, 2010; Wilson et al., 2013b), the neurotransmitters and neuromodulators of itch (Kardon et al., 2014; Mishra and Hoon, 2013; Sun and Chen, 2007), and especially the itch-mediating neurons and neurocircuits (Bourane et al., 2015; Han et al., 2013; Huang et al., 2018; Mishra and Hoon, 2013; Roberson et al., 2013; Ross et al., 2010; Sun et al., 2009, 2017). Primary sensory neurons, especially nociceptors, express TRPA1 for pain sensation and sensitization (Bautista et al., 2006; Patapoutian et al., 2009; Story et al., 2003). TRPA1 is also expressed by pruriceptive neurons (pruriceptors) and regulates acute and chronic itch (Liu et al., 2013; Wilson et al., 2011, 2013a). TRPA1 was regarded as a key signaling molecule for pruritus instead of a receptor of itch, because it is coupled with G-protein-coupled receptors such as MrgprA3 and serotonin receptor HTR7 that can be directly activated by pruritogens (Liu et al., 2009; Morita et al., 2015; Wilson et al., 2011). Although TRPA1 regulates both pain and itch, allyl isothiocyanate (AITC), the most utilized agonist of TRPA1, was thought to primarily elicit pain after intradermal injection (Ross, 2011). It is unclear whether direct activation of TRPA1 causes itch. Most known agonists of TRPA1, such as pungent natural compounds and environmental irritants covalently bind cysteine residues at the intracellular C-terminal of TRPA1 (Macpherson et al., 2007; Paulsen et al., 2015). However, extracellular activation of TRPA1 remains unclear. It is also unknown whether a miRNA can bind and activate an ion channel.

Cutaneous T cell lymphomas (CTCL) are the most common primary skin lymphomas (Bradford et al., 2009; Ralfkiaer et al., 2011), and patients with CTCL frequently complain of severe itching (Field et al., 2016). Notably, several microRNAs (miRNAs), including miR-21, miR-155, miR-326, and miR-711, are upregulated in skin biopsies from the lymphoma patients (Ralfkiaer et al., 2011; Sandoval et al., 2015). We developed a new mouse model of CTCL by intradermal inoculation of human Myla cells. In this model, mice developed lymphoma and chronic itch, which is associated with increased serum levels of hsa-miR-711 released from inoculated human cancer cells. Using a cheek model that can distinguish pain (wiping) and itch (scratching) (Shimada and LaMotte, 2008), we find that intradermal injection of miR-711 induces scratching but not wiping. Furthermore, miR-711 binds to TRPA1 via the core sequence GGGACCC to activate TRPA1 at the extracellular S5-S6 loop. Finally, miR-711 is both sufficient and required for driving chronic itch in the CTCL model.

RESULTS

miR-711 Elicits Pruritus via Specific Core Sequence and TRPA1

We searched for miRNAs that are dysregulated in patients with lymphoma. Upregulations of miR-21, miR-155, miR-326, and miR-711 were reported in skin biopsies from the lymphoma patients (Ralfkiaer et al., 2011; Sandoval et al., 2015). Next, we tested whether the dysregulated miRNAs are capable of inducing itch or pain in naive animals following intradermal injection (1 mM, 5 μ L) using the cheek model that can distinguish pain versus itch (Shimada and LaMotte, 2008). Notably, among 4 miRNAs we tested, only miR-711, but not miR-21, miR-155, and miR-326, evoked marked scratching in naive mice (Figures 1A). Pruritus evoked by intradermal miR-711 is dose dependent: mild but significant scratching was evident at 0.01 and 0.1 mM ($p < 0.001$, Figure S1A). At the highest dose (5 mM, 5 μ L) we tested, intradermal miR-711 resulted in a very strong scratching with 395.2 ± 32.8 bouts per hour. This severe pruritus resulted in skin lesion at the injection site (Figures S1A and S1B). Thus, miR-711 is a highly potent pruritogen. The onset of miR-711-induced pruritus was very rapid, with a shorter latency than that induced by the classic pruritogens chloroquine (CQ) and histamine (Figure S1C), suggesting that miRNA may trigger pruritus through different mechanisms. Despite severe pruritus, intradermal cheek injection of miR-711 failed to evoke pain (wiping) at all the concentrations we tested (Figures 1A and S1A). Neither did intradermal miR-21, miR-155, and miR-326 elicit wiping behavior (Figure 1A). We also examined miRNA-induced itch using the back model, as the cheek skin and back skin are differentially innervated by trigeminal ganglion (TG) and DRG sensory neurons. Intradermal injection of miRNA-711 (0.01–1 mM, 10 μ L) on the nape of neck also induced dose-dependent scratching, whereas miR-21, miR-155, and miR-326 had no effects (Figures S1E and S1F).

How does miR-711 induce itch? TRPA1 and TRPV1 are expressed by pruriceptive and nociceptive DRG neurons and regulate acute and chronic pruritus (Kittaka et al., 2017; LaMotte et al., 2014; Wilson et al., 2011, 2013a). Given the fast onset of the miR-711-induced pruritus, we reasoned that miR-711 might trigger

itch via direct or indirect activation of TRP channels on sensory neurons. miR-711-induced acute itch was abrogated in *Trpa1*^{-/-} but not *Trpv1*^{-/-} mice (Figure 1B). Pruriceptive neurons also expressed TLR7, which induces pain or itch by coupling to TRPA1 (Liu et al., 2010; Park et al., 2014). However, miR-711-induced pruritus was unaltered in *Tlr7*^{-/-} mice (Figure 1B). Thus, miR-711 evokes itch via TRPA1 but not TRPV1 and TLR7.

Does miRNA induce itch via specific sequence? Figure 1C shows the sequences of different miRNAs we tested in Figure 1A. A comparison of mouse and human miR-711 sequence revealed that mmu-miR-711 and hsa-miR-711 contain the same core sequence GGGACCC and both miRNAs from different species were able to evoke pruritus (Figures 1A and S1D). A miRNA database (miRBase) search showed that hsa-miR-642b-3p also contains the core sequence GGGACCC, and consistently, intradermal hsa-miR-642b-3p resulted in pruritus too (Figure 1A). Like mouse miR-711, hsa-miR-711 and hsa-miR-642b-3p failed to elicit wiping at the concentration that can produce scratching (Figure 1A).

To determine the specific sequence of miR-711 that is critical for pruritus, we generated 6 mutants of miR-711 (m1 to m6) by converting several nucleotides to adenosine (Figure 1D) and tested their effects on pruritus. Mutations on the first seven nucleotides in m1, m2, and m6 resulted in marked reduction in scratching, suggesting that GGGACCC is the core sequence for eliciting pruritus (Figure 1E). Importantly, this core sequence was sufficient to elicit scratching but not wiping, whereas the mutant oligonucleotides (AAAAAAA) did not affect pain and itch (Figure 1F).

Next, we examined whether AITC and miRNA-711 produce distinct pain or itch. Intradermal and cheek administration of AITC at high concentrations (5 and 10 mM, 5 μ L) induced wiping but not scratching. Interestingly, low concentrations of AITC (10 and 100 μ M) induced mild itch but no pain, whereas a medium concentration (1 mM) induced both scratching and wiping (Figures 1A and S1A). This finding suggests that AITC produces both pain and itch in a dose-dependent manner. We also tested mechanical and thermal pain sensitivity in a hind paw. Intraplantar injection of miR-711, at the concentration that can elicit itch (1 mM), failed to induce heat hyperalgesia and mechanical allodynia. In contrast, intraplantar AITC elicited marked hyperalgesia and allodynia (Figures 1G and 1H).

Neurogenic inflammation is a unique form of inflammation arising from the release of inflammatory mediators from primary afferent neurons (Ji et al., 2014). Intraplantar injection of capsaicin (1 mM) and AITC (5 mM) elicited robust neurogenic inflammation in hind paws, as revealed in the Evans blue test. However, intraplantar administration of miR-711 (1 mM) failed to elicit neurogenic inflammation (Figures 1I and 1J).

Collectively, these results indicate that miR-711 and AITC differently regulate pain, itch, and neurogenic inflammation.

miR-711 Activates TRPA1 in Heterologous Cells to Elicit Inward Currents and Single Channel Activities

To investigate whether miR-711 directly activates TRPA1, we assessed the function of TRPA1 by conducting patch-clamp recordings in heterologous cells. Bath application of miR-711, but not miR-21, miR-155, and miR-326 (10 μ M), produced

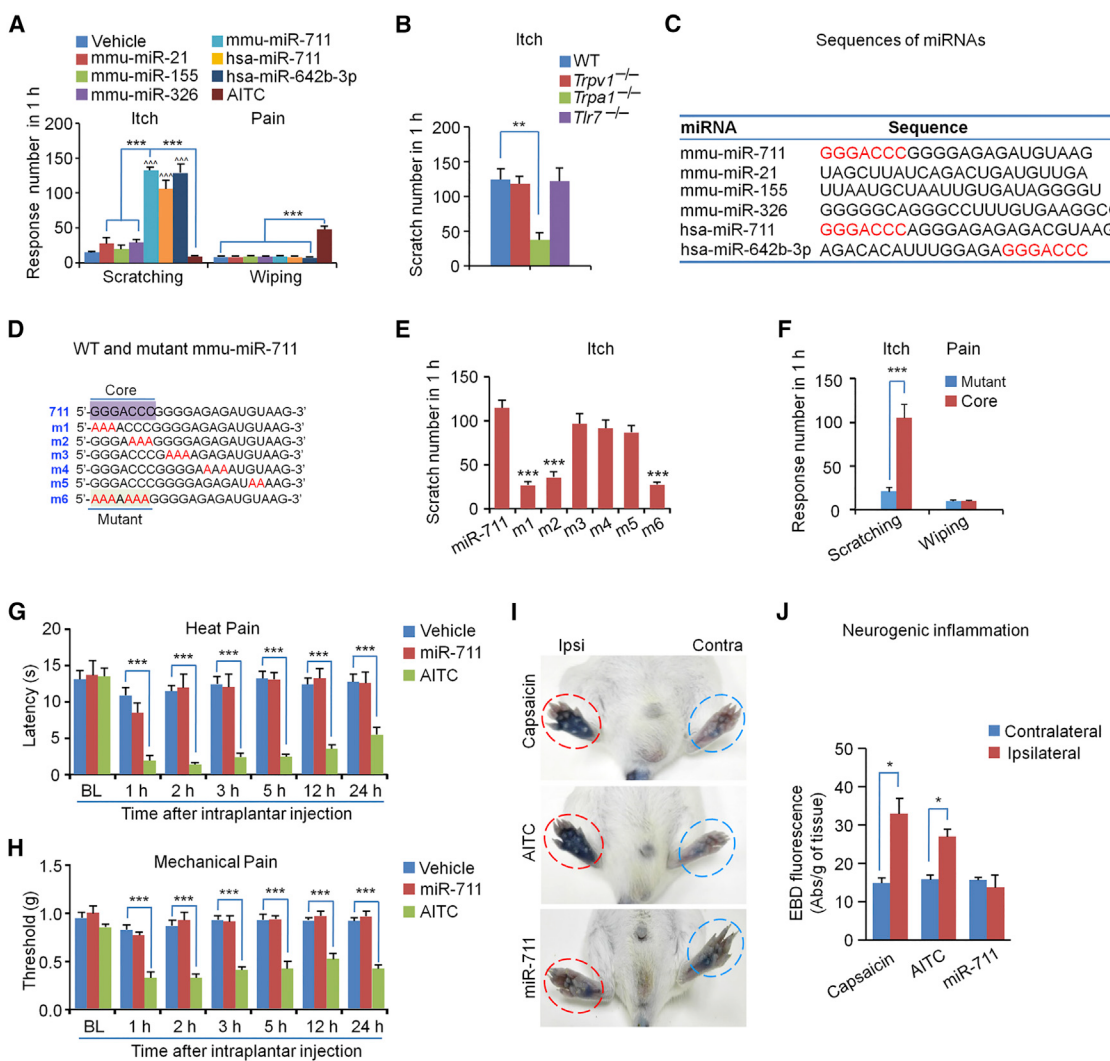


Figure 1. Intradermal miR-711 Induces Itch but Not Pain via the GGGACCC Core Sequence and TRPA1

(A) Intradermal cheek injection of GGGACCC containing miRNAs (mmu-miR-711, has-miR-711, and has-miR-642b-3p), but not mmu-miR-21, mmu-miR-155, and mmu-miR-326, all at 1 mM (5 μ L), induces scratching but not wiping in naive mice. Intradermal injection of AITC at a high concentration (10 mM, 5 μ L) induces wiping but not scratching. $^{***}p < 0.001$, versus vehicle, $^{**}p < 0.01$, one-way ANOVA, $n = 5\text{--}7$ mice/group.

(B) mmu-miR-711-induced scratching is reduced in *Trpa1*^{-/-} but not *Trpv1*^{-/-} and *Tlr7*^{-/-} mice. $^{**}p < 0.01$, versus WT, one-way ANOVA, $n = 5\text{--}6$ mice/group.

(C) Sequences of the miRNAs tested in this study. The core sequence of these miRNAs is highlighted in red.

(D) Sequences of mmu-miR-711 and 6 mutants of mmu-miR-711 (m1 to m6). The mutated nucleotides are highlighted in red.

(E and F) The core sequence GGGACCC is both required and sufficient for miR-711 to induce pruritus.

(E) Scratching induced by intradermal injection of mmu-miR-711 and its mutants (1 mM, 5 μ L). $^{***}p < 0.001$, versus miR-711, one-way ANOVA, $n = 5\text{--}10$ mice/group.

(F) The core sequence GGGACCC but not mutant sequence AAAAAAA is sufficient to elicit scratching not wiping in naive mice. $^{***}p < 0.01$, two-tailed Student's t test, $n = 5$ mice/group.

(G and H) Intraplantar injection of AITC (10 mM, 10 μ L) but not miR-711 (1 mM, 10 μ L) elicits heat hyperalgesia (G) and mechanical allodynia (H). $^{***}p < 0.001$, two-way ANOVA, $n = 5$ mice/group.

(I and J) Intraplantar injection of AITC (5 mM, 10 μ L) and capsaicin (1 mM, 10 μ L) but not miR-711 (1 mM, 10 μ L) induces neurogenic inflammation in a hindpaw, as measured by Evans blue test.

(I) Images of hind paws with Evans blue staining. Ipsi, ipsilateral paws; Contra, contralateral paws.

(J) Quantification of Evans blue staining in ipsilateral and contralateral hind paws. $^*p < 0.05$, two-tailed Student's t test, $n = 5\text{--}6$ mice/group.

Data are represented as mean \pm SEM. See also Figure S1.

inward currents in *Trpa1*-expressing HEK293 cells (Figures 2A and 2B). AITC (50 μ M) also induced inward currents in these cells (Figures 2A and 2B). The second application of miR-711 did not

induce obvious desensitization of TRPA1 (Figures S2A and S2B). A967079, a selective TRPA1 antagonist (10 and 50 μ M) dose-dependently blocked the miR-711-evoked currents

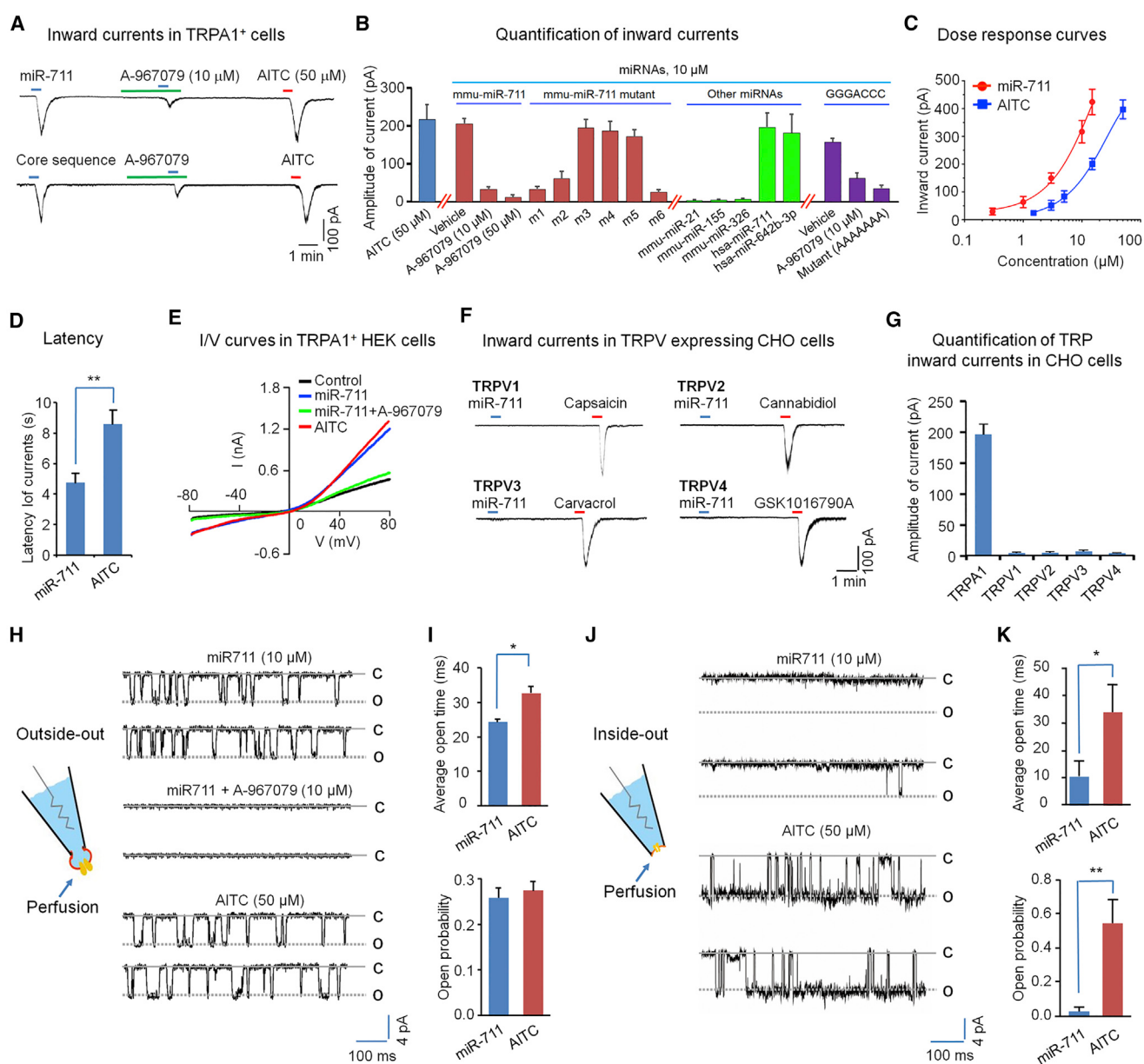


Figure 2. miR-711 Activates TRPA1 in Heterologous Cells

(A–E) mmu-miR-711 induces inward currents in HEK293 cells expressing hTRPA1.

(A) Traces of inward currents induced by mmu-miR-711 and the core sequence. Note that the induced currents are blocked by A967079 (10 μM).

(B) Quantification (amplitude) of inward currents induced by AITC (50 μM), miRNAs (10 μM), core sequence, mutant RNA oligos (10 μM), and the effects of A967079 (10 and 50 μM). n = 6–11 cells/group.

(C) Dose-response curves comparing the amplitudes of inward currents induced by mmu-miR-711 and AITC. n = 5–11 cells/group.

(D) Latency of the inward currents evoked by AITC (50 μM) and mmu-miR-711 (10 μM) after bath perfusion. **p < 0.01, two-tailed Student's t test, n = 7–8 cells/group.

(E) I/V curves elicited by mmu-miR-711 (10 μM), AITC (100 μM), and mmu-miR-711 + A967079 (10 μM). n = 5 cells for each condition.

(F and G) mmu-miR-711 (10 μM) fails to evoke inward currents in CHO cells transfected with mouse *Trpv1*, *Trpv2*, *Trpv3*, and *Trpv4* cDNAs.

(F) Traces of inward currents induced by the agonists of TRPV1 (capsaicin, 50 nM), TRPV2 (cannabidiol, 100 μM), TRPV3 (carvacrol, 300 μM), and TRPV4 (GSK1016790A, 1 μM) but not by mmu-miR-711 (10 μM).

(G) Quantification of inward currents described in (F). n = 5–7 cells/group.

(H and I) Single channel activities induced by bath application of AITC (50 μM) and mmu-miR-711 (10 μM) in outside-out patch recordings (held at -60 mV) in membrane excised from hTRPA1-expressing HEK293 cells.

(H) Traces of single-channel activities. Left, schematic of outside-out patch recording.

(I) Quantification of single channel open time (top) and open probability (bottom). *p < 0.05, Two-tailed Student's t test, n = 5 patches from 5 cells per group.

(legend continued on next page)

(Figures 2A and 2B). A dose-response analysis revealed that miR-711 is more potent than AITC for inducing TRPA1 activation, as indicated by a left-shift of the dose-response curve (Figure 2C). Of interest, the latency of miR-711-induced inward currents is shorter than that of AITC (Figure 2D), implicating a faster action of miR-711. The miR-711-evoked current had a current-voltage relationship consistent with TRPA1 activation, with a reversal potential of 0 mV and outward rectification (Figure 2E). By contrast, miR-711 failed to trigger inward currents in CHO cells that express *Trpv1*, *Trpv2*, *Trpv3*, and *Trpv4*, suggesting that miR-711 specifically acts on TRPA1 (Figures 2F and 2G).

To validate that miR-711 directly activates TRPA1 on the cell surface, we carried out single channel recordings in HEK293 cells expressing TRPA1. Outside-out patch recordings showed that bath application of miR-711 and AITC on the extracellular surface each elicited single-channel opening events (Figure 2H). The miR-711-induced single channel activity was completely blocked by A967079 (Figure 2H). Interestingly, the duration of the miR-711-evoked single channel opening (average open time) but not the open probability, and conductance was significantly shorter ($p < 0.05$) than that evoked by AITC (Figure 2I and Figure S2C). Inside-out patch recordings in *Trpa1*-expressing HEK293 cells showed that bath application of AITC but not miR-711 on the intracellular surface elicited single-channel opening events (Figures 2J and 2K). Thus, unlike AITC, miR-711 activates TRPA1 on the extracellular side.

miR-711 Activates a Subpopulation of Sensory Neurons Reminiscent of Pruriceptors

To determine the neuronal population activated by miR-711, we performed calcium imaging on cultured DRG neurons isolated from Pirt-GCaMP3 mice (Anderson et al., 2018). We found that 10 μ M miR-711 did not evoke meaningful calcium signaling, although this concentration was sufficient to induce inward currents in TRPA1-expressing HEK293 cells. At 50 μ M, miR-711 caused Ca^{2+} increase in 3.9% DRG neurons ($n = 544$ neurons from 3 mice, Figures 3A and 3B). After miR-711 stimulation, we sequentially stimulated the same DRG neurons with histamine (500 μ M), chloroquine (CQ, 1,000 μ M), and AITC (200 μ M). In 544 neurons we analyzed, 5.5%, 5.1%, and 22.6% neurons showed responses to histamine, CQ, and AITC, respectively (Figure 3C). For the miR-711-responsive neurons, majority of them also showed responses to CQ (66.7%) and histamine (61.9%), and all of them responded to AITC (Figures 3A–3C). As expected, miR-711 (50 μ M) also evoked calcium responses in TRPA1-expressing HEK293 cells (Figures S3A and S3B). Notably, A967079 completely blocked the miR-711-evoked calcium responses in DRG neurons, confirming a specific activation of TRPA1 by miR-711 (Figures S3C–S3E).

We also examined calcium responses in TG neurons isolated from Pirt-GCaMP3 mice. Interestingly, compared with DRG neu-

rons, TG neurons showed greater responses to miR-711, pruritogens, and AITC: 12.3% (25/204) of TG neurons responded to miR-711 (50 μ M), and 6.9%, 9.3%, and 32.4% neurons exhibited respective responses to histamine, CQ, and AITC. Among the miR-711-responsive neurons, the majority of them also showed responses to CQ (76%) and histamine (52%), and all (100%) to AITC (Figures S3F–S3H). Collectively, our calcium imaging data indicate that miR-711 activates a subset of TRPA1⁺ sensory neurons in mice.

miR-711 and AITC Cause Distinct Activation of TRPA1 in Mouse DRG Neurons

To further assess distinct neuronal activation by miR-711 and AITC, we conducted electrophysiology to record inward currents and action potentials in small-diameter DRG neurons (<25 μ m). Exposure of dissociated DRG neurons to exogenous miR-711 (10 μ M) induced rapid inward currents, which were blocked by A-967079 and abolished in *Trpa1* knockout mice (Figures 4A and 4B). miR-711 (10 μ M) also induced action potentials in small-diameter DRG neurons, and this excitation was lost in TRPA1-deficient neurons (Figures 4C and 4D), suggesting that miR-711 is sufficient to excite sensory neurons via TRPA1. Notably, 16.7% (15/90) and 11.5% (15/130) small-diameter neurons responded to AITC and miR-711, respectively, with inward currents or action potentials. Thus, miR-711-respoinding neurons could be a subset of TRPA1⁺ neurons. Additional action potential analysis revealed that compared with AITC, miR-711 elicited action potentials with a shorter duration, but the after-hyperpolarization of the action potentials did not differ after these treatments (Figures 4D and 4E). It was shown that AITC increased calcium permeability (Bobkov et al., 2011; Karashima et al., 2010). I/V and reversal potential analysis revealed that compared to AITC, miR-711 had lower permeability to Ca^{2+} but similar permeability to Na^+ in *Trpa1*-expressing HEK293 cells (Figures S2D and S2E). The resting membrane potentials (RMPs) of the recorded neurons are near -60 mV, indicating their healthy conditions (Figure S4A). Our data suggest that distinct TRPA1 activation by miR-711 and AITC may underlie their distinct sensory behaviors (itch versus pain).

Since miR-711 at 10 μ M induced inward current but no calcium response in DRG neurons, we also assessed whether miR-711 would inhibit calcium channel activities. No evidence was found to support this notion: miR-711 at 10 μ M did not alter calcium currents in DRG neurons (Figures S4B–S4D).

We also tested the actions of miRNAs in human DRG neurons from donors (Chang et al., 2018). Given the shared core sequence of mouse and human miR-711, we predicted that human DRG neurons should also respond to hsa-miR-711. As shown in Figure S4E, hsa-miR-711 (10 μ M) evoked TRPA1-dependent inward currents in human DRG neurons.

(J and K) Single channel activities induced by bath application of AITC (50 μ M) and mmu-miR-711 (10 μ M) in inside-out patch recordings (held at -60 mV) in membrane excised from hTRPA1-expressing HEK293 cells.

(J) Traces of single-channel activities. Left, schematic showing inside-out patch recording.

(K) Quantification of single channel open time (top) and open probability (bottom). * $P < 0.05$, ** $p < 0.01$, two-tailed Student's t test, $n = 6$ patches from 6 cells per group.

Data are represented as mean \pm SEM. See also Figure S2.

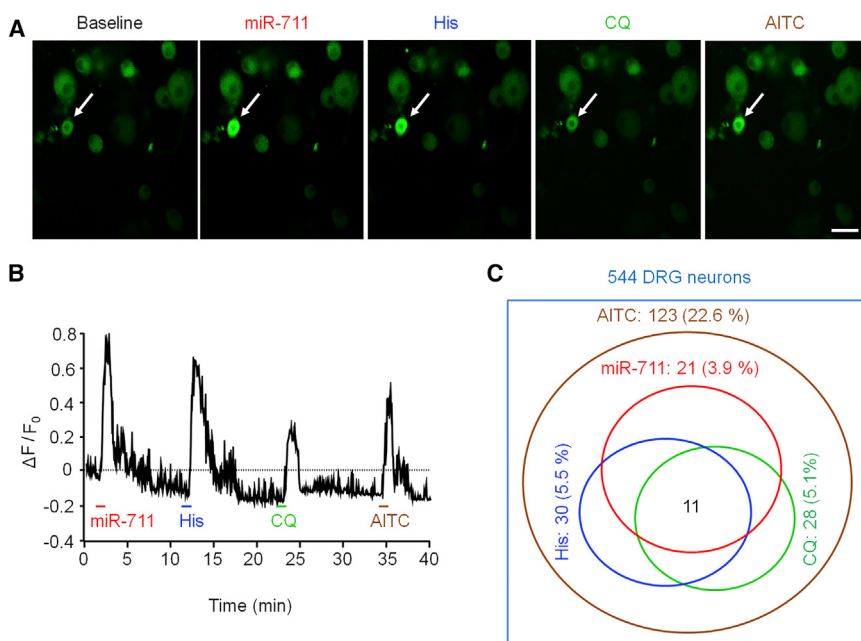


Figure 3. Calcium Imaging in DRG Cultures Showing Activation of a Subset of TRPA1-Expressing Sensory Neurons by miR-711 in Pirt-GCaMP3 Mice

(A) Representative images of calcium responses to mmu-miR-711 (50 μ M), histamine (His, 500 μ M), chloroquine (CQ, 1,000 μ M), and AITC (200 μ M) sequentially. Scale, 50 μ m.

(B) Representative traces show a neuronal calcium response to mmu-miR-711 (50 μ M), Histamine (His, 500 μ M), CQ (1,000 μ M), and AITC (200 μ M).

(C) Venn diagram showing overlaps between miR-711-responsive neurons and histamine (His)-, CQ-, and AITC-responsive neurons and the percentage of each population in cultured DRG neurons. A total of 544 neurons from 3 mice were analyzed, and 11 neurons respond to all the stimuli. See also Figure S3.

Furthermore, hsa-miR-642b-3p, which contains the GGGACCC core sequence and is capable of inducing scratching in mice (Figures 1A and 1C), induced similar inward currents on human DRG neurons as hsa-miR-711 (Figures S4E and S4F). The fact that certain miRNAs can activate human sensory neurons highlights a translational potential of this study.

miR-711 Core Sequence Binds to TRPA1 at Specific Residues

In order to explore the binding modes of miR-711 core sequence GGGACCC to TRPA1 ion channel, we performed extensive replica exchange discrete molecular dynamics simulations (RexDMD) (Dokholyan et al., 1998; Shirvanyants et al., 2012), starting from the cryo-electron microscopy coordinates of TRPA1 (Paulsen et al., 2015) and the structural model of GGGACCC generated using iFoldRNA (Sharma et al., 2006). We estimated the binding energies between miRNA and TRPA1 along the entire simulations and collected the ensemble of high-affinity GGGACCC/TRPA1 conformations (i.e., energy lower or equal than -75 kcal/mol, Figures 5A–5D and Figures S5A–S5C). The representative high-affinity and stable binding mode of GGGACCC to human TRPA1 complex is represented in Figures 5A and 5B, while the frequencies of contacts between TRPA1 residues and GGGACCC motif are summarized in Figure 5C. Because miR-711 has a shared core sequence in different species (Figure S1D), we postulate that TRPA1 residues interacting with miR-711 should be conserved in mouse and human TRPA1 (mTRPA1 and hTRPA1). Sequence alignment of human, mouse, and rat TRPA1 showed that the predicted amino acid residues with possible interactions with GGGACCC are classified into three categories: non-conservative sites with different properties, conservative sites with similar properties, and ultra-conservative sites with identical amino acids (Figure S6A). Figure 5A shows the proximity of

the GGGACCC core sequence with the Subunit 1, 2, and 3 of hTRPA1. The hTRPA1 residues interacting with individual nucleotides of GGGACCC were also highlighted in Figures 5B and

Figures S5D–S5K, with special focus on P934 of hTRPA1 (Figures 5B and 5C).

miR-711 Activates mTRPA1 at P937 of the S5-S6 Extracellular Loop

AITC binds the intracellular ankyrin repeats at the N-terminal of TRPA1 (Macpherson et al., 2007; Paulsen et al., 2015). We predicted that miR-711 might interact with TRPA1 at extracellular sites, given the hydrophilic nature of miRNAs. This prediction is also consistent with the result from computer simulation (Figures 5A–5D). According to the prediction in Figure 5C and amino acid sequence alignment in Figure S6A, we generated 8 mutations on the predicted and highly conserved sites in mTRPA1: one in S1-S2 loop (M1), one in S3-S4 loop (M4), and six in S5-S6 (M7, M8, M9, M10, M11, M12), which are illustrated in Figures S6B and S6C. We also generated 4 mutations in the extracellular loop of mTRPA1 (M2, M3, M5, M6). In addition, we produced mutant M13, containing one mutation on predicted and non-conservative site Y⁹³⁶, one mutation on predicted and ultra-conservative site P⁹³⁷, and one mutation on non-predicted site L⁹³⁹ (Figures S6B and S6C). We excluded those mutations that caused marked disruption of TRPA1 structure and function based on loss of AITC responses. Notably, mutants M1, M6, M7, M8, M9, and M12 showed substantial reductions in both AITC and miR-711 induced currents (Figures 5E, S6B, and S6C).

To assess the specific changes evoked by miR-711, we focused on the remaining TRPA1 mutants, in which AITC-induced currents were unaltered, including M2, M3, M4, M5, M10, M11, and M13 (Figures 5E–5G, S6B and S6C). Strikingly, miR-711-evoked currents were markedly reduced in M11 after a single residue mutation of mP937 (equivalent to hP934) at the S5-S6 extracellular loop (Figures 5E–5G, S6B, and S6C). Potential interactions of hP934 with nucleotides G003 and A004 are illustrated in Figures 5B, 5C, and S5D–S5K. As expected, M13

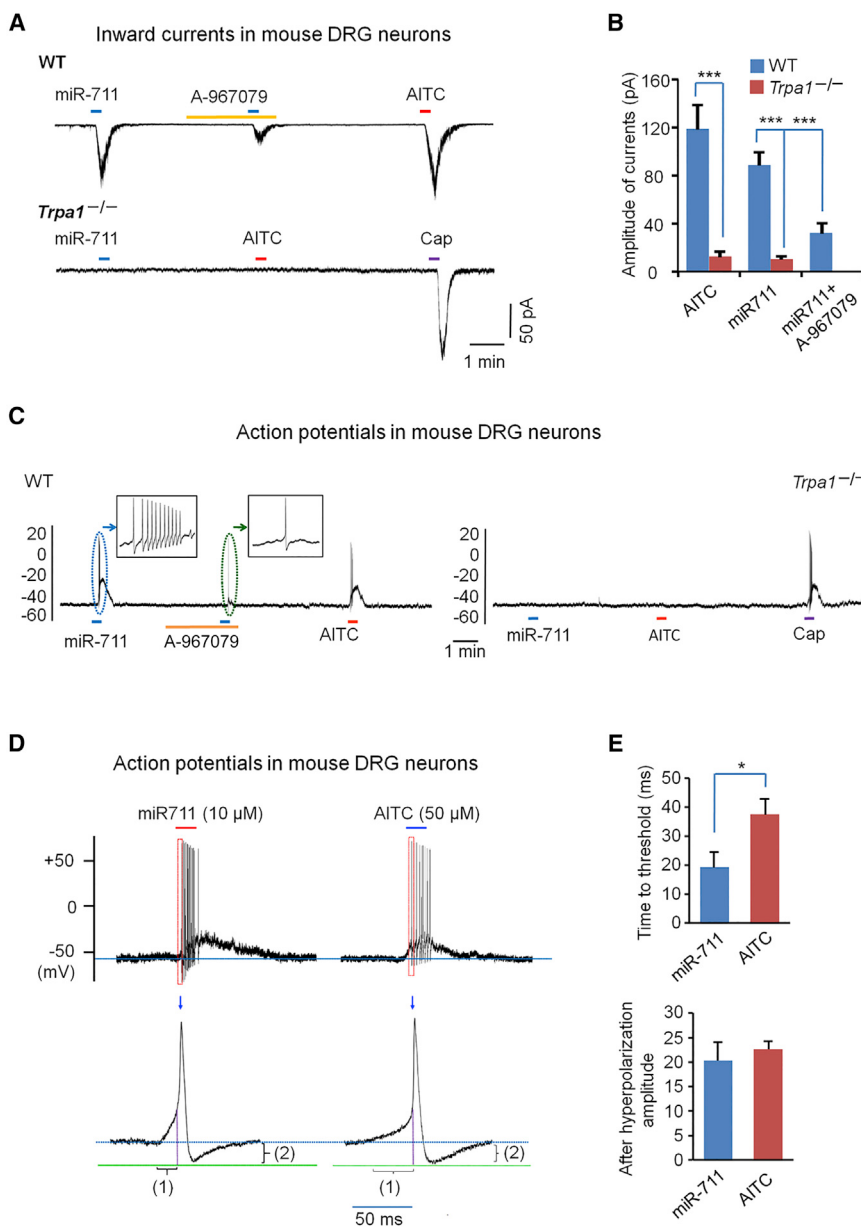


Figure 4. miR-711 Induces Inward Currents and Action Potentials via TRPA1 in Mouse DRG Neurons

(A and B) Inward currents induced by miR-711 and AITC in small-diameter DRG neurons in WT and *Trpa1^{-/-}* mice. Cap, capsaicin. (A) Traces of inward currents. Note that miR-711-induced inward currents are blocked by A967079 (10 μM) and abolished in *Trpa1^{-/-}* mice.

(B) Amplitude of inward currents. ***p < 0.001, two-tailed Student's t test, n = 7–8 neurons/group.

(C) Action potentials induced by miR-711 and AITC in small-diameter mouse DRG neurons in WT and *Trpa1^{-/-}* mice. Note that miR-711-induced action potentials are blocked by A967079 (10 μM) and abolished in *Trpa1^{-/-}* mice. n = 10–15 neurons/group. Cap, capsaicin.

(D and E) Distinct action potentials induced by miR-711 and AITC in small-diameter DRG neurons in WT mice.

(D) Traces of the action potentials. Single action potentials in the red boxes are enlarged in the lower panels.

(E) Quantification of the action potential's rising time or time to threshold, indicated as (1) in (D) and after hyperpolarization amplitude, indicated as (2) in (D). *p < 0.05, two-tailed Student's t test, n = 7–9 neurons/group.

Data are represented as mean ± SEM. See also Figure S4.

with triple mutations (Y936, P937, and L939), including M11 single mutation at P937, resulted in further reduction in miR-711 current (Figures 5E–5G, S6B, and S6C), suggesting that the adjacent residues (Y936 and L939 of mTRPA1, equivalent to H933 and L936 of hTRPA1) may also interact with the core sequence to regulate TRPA1 function. In contrast, M2, M3, M4, M5, and M10 had no effects on either AITC or miR-711 induced currents (Figures S6B and S6C). Collectively, these results show that extracellular residues, especially P937, can interact with the core sequence to regulate TRPA1 activation by miR-711.

Interaction of miR-711 and TRPA1 Is Required for miR-711 to Elicit Itch

To assess the interaction of miR-711 and TRPA1, we also conducted an RNA binding assay using biotin-conjugated miR-

711, which was able to pull down TRPA1 (Figure 6A). By contrast, the mutant miR-711 (m6) only showed weak binding activity to TRPA1 (Figure 6A) and failed to elicit itch (Figure 1E). Competing experiment confirmed that wild-type but not mutant miR-711 (m6) inhibited the binding of biotin-labeled miR-711 to TRPA1 (Figures 6B and 6C). We also tested the miRNA/TRPA1 interaction in native mouse neurons by incubating DRG neuronal cultures with Cy3-labeled miR-711. Immunofluorescence revealed that Cy3-labeled miR-711 but not Cy3-

labeled mutant oligo (m6) binds to TRPA1 on the cell surface. However, TRPA1-negative DRG neurons show no binding to Cy3-labeled miR-711 (Figure 6D).

To determine a physiological relevance of the miR-711/TRPA1 interaction, we investigated whether blocking the interaction would affect itch. To this end, we designed a small blocking peptide, FRNELAPVPVLTFQL, which covers the underlined residues Y936, P937, and L939 in the S5-S6 loop of mTRPA1, as well as other potentially interacting residues in Subunit-1 of TRPA1 (Figures 5B and 5C). Notably, the blocking peptide disrupted the miR-711/TRPA1 interaction (Figure 6E) and suppressed the miR-711-induced TRPA1 currents in *Trpa1*-expressing HEK293 cells (Figures 6F and 6G). Importantly, intra-dermal injection of the blocking peptide prevented the miR-711-induced pruritus (Figure 6H). In contrast, the blocking

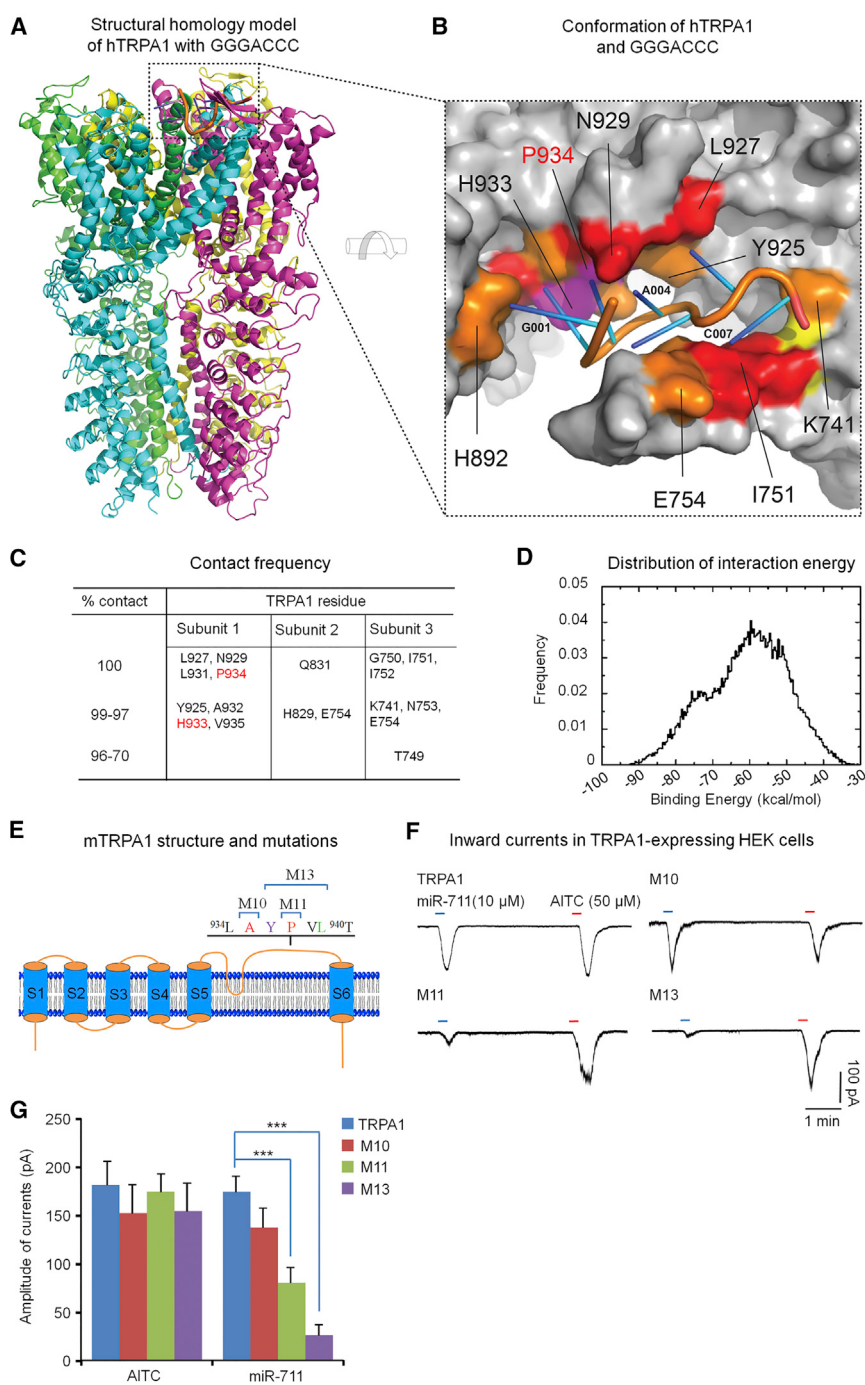


Figure 5. Computer Simulation of miR-711 Core Sequence Binding to the Extracellular Loops of hTRPA1 and Identification of the Binding Sites

(A) Structure of the core sequence GGGACCC bound to hTRPA1 extracellular surface. The represented pose is the lowest estimated binding energy structure (i.e., -87 kcal/mol) extracted from the most populated cluster of high-affinity GGGACCC/TRPA1 conformations. The bound conformation of GGGACCC (labeled in orange) spans over three monomers of the channel, namely subunit 1, 2, and 3, as represented by green, cyan, and magenta cartoons, respectively.

(B) Zoomed view of GGGACCC bound to TRPA1 extracellular surface. The hit map on TRPA1 surface represents the contact frequency between TRPA1 residues and GGGACCC in the most populated ensemble of high-affinity GGGACCC/TRPA1 conformations (i.e., estimated binding energy equal or lower than -75 kcal/mol). TRPA1 residues contacting GGGACCC with frequency of 100%, 97%–99%, and 70%–96% are revealed as red, orange, and yellow surface, respectively. All of the other TRPA1 residues are represented with a gray surface. Residues that upon mutation to alanine selectively disrupt the miRNA711-mediated activation of TRPA1 are represented as magenta surface. G001 and C007 indicate the first and last nucleotide of the core sequence, respectively.

(C) Contact frequencies between hTRPA1 residues and GGGACCC. The frequencies of contacts are extracted from the most populated cluster of high-affinity GGGACCC/TRPA1 conformations. The TRPA1 residues that upon mutation to alanine selectively disrupt the GGGACCC-mediated activation of hTRPA1 are shown in red.

(D) Distributions of GGGACCC estimated binding energies to hTRPA1 collected over a 2 million-step RexDMD simulation. The left shoulder of the distribution, starting at binding energy equal to -75 kcal/mol, characterizes the conformational ensemble of high-affinity GGGACCC/TRPA1 complex.

(E) Schematic diagram of hTRPA1 with detailed residues for Subunit 1. Purple, red, and green residues indicate predicted but non-conservative Y936, predicted and ultra-conservative P937, and non-predicted L939, respectively, on the S5-S6 loop. Black residues are non-mutated sites.

(F and G) mmu-miR-711 and AITC induce inward currents in CHO cells transfected with wild-type and mutant mmu-Trpa1 cDNAs (M10, M11, M13).

(F) Traces of inward currents induced by mmu-miR-711 on CHO cells expressing mmu-TRPA1 or its mutants.

(G) Quantification of AITC and mmu-miR-711 induced currents. *** $p < 0.001$, one-way ANOVA, $n = 8$ –15 cells/group. Note that mutations M11 and M13 disrupt miR-711 but not AITC-induced currents.

Data are represented as mean \pm SEM. See also Figure S5.

peptide did not affect the AITC-induced inward current (Figures 6F and 6G) and had no effect on acute itch induced by compound 48/80 and chloroquine (Figure 6H), implying that the effects of the blocking peptide are specific for miR-711. In a con-

trol experiment, we also designed a mutated peptide, with mutations in 3 residues underlined (FRNELAAAVATFGQL, Figure 6E). Neither did this mutated peptide block the miR-711/TRPA1 interaction, nor did this peptide inhibit the miR-711-induced inward

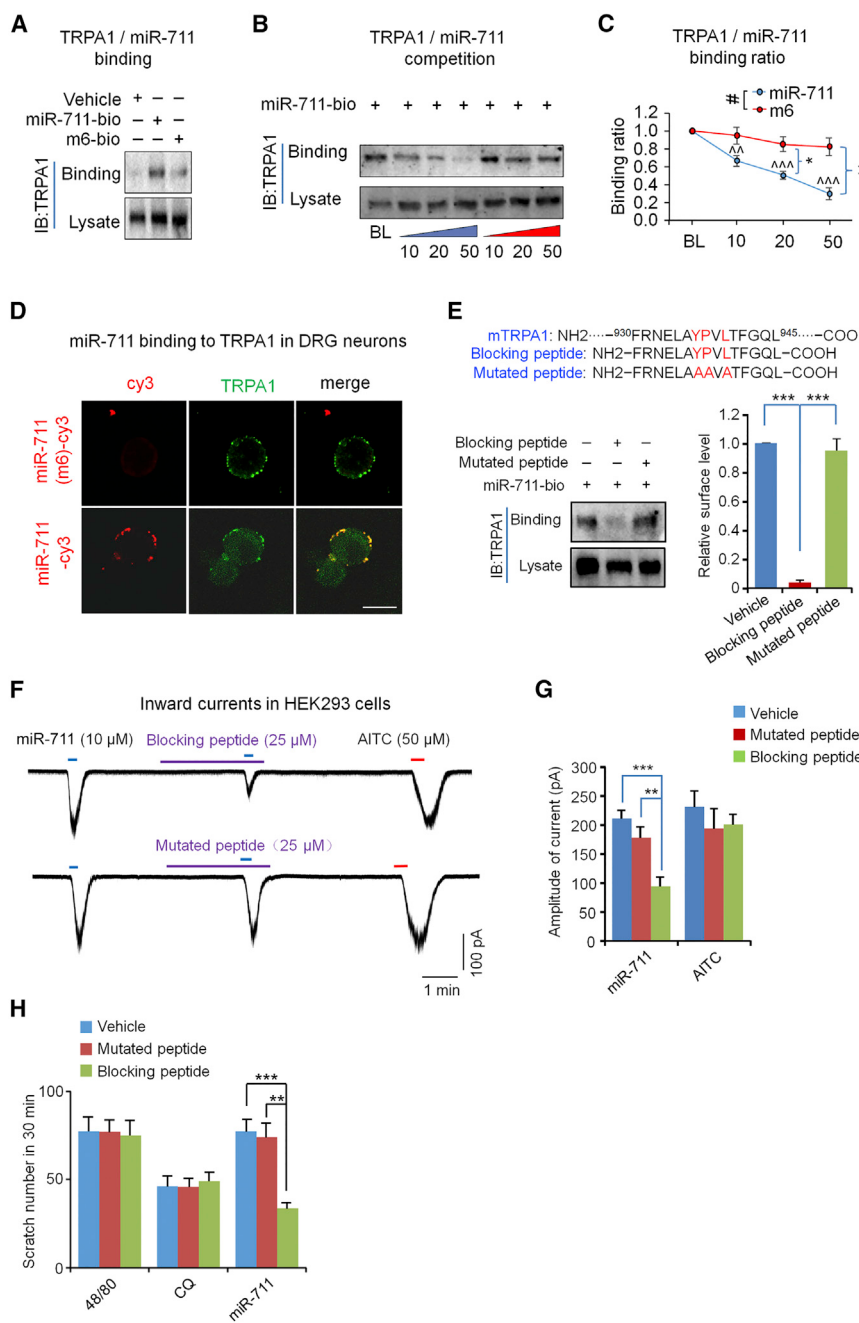


Figure 6. Disruption of miR-711/TRPA1 Interaction with a Blocking Peptide Reduces Itch

(A–D) Interaction between miR-711 and TRPA1. (A) RNA pull-down assay shows strong hTRPA1 binding to biotin (bio)-conjugated mmu-miR-711 but weak hTRPA1 binding to bio-mmU-miR-711 (m6).

(B) RNA pull-down shows that wild-type mmu-miR-711 (blue) but not mutant mmu-miR-711 (m6, red) competes with bio-mmU-miR-711 for the binding to hTRPA1. miR-711 (10–50 μ M, blue) or mutant miR-711 (m6, 10–50 μ M, red) were added 15 min before the incubation with biotin-conjugated miR-711 (10 μ M).

(C) Quantification of mmu-miR-711/hTRPA1 binding activity shown in (B). $^{\wedge}p < 0.01$, $^{\wedge\wedge}p < 0.001$, versus control (no treatment), one-way ANOVA, $*p < 0.05$, $^{**}p < 0.01$, $^{***}p < 0.05$, miR-711 versus m6, two-way ANOVA, $n = 5$ experiments.

(D) Live cell labeling shows the binding of Cy3-labeled mmu-miR-711 but not Cy3-labeled mmu-miR-711 (m6) to mTRPA1 on the surface of cultured DRG neurons. Scale, 20 μ m.

(E–H) A blocking peptide disrupts mmu-miR-711/hTRPA1 interaction and mmu-miR-711-induced currents and pruritus.

(E) RNA pull-down assay showing disruption of the mmu-miR-711/hTRPA1 interaction by the blocking peptide but not by the mutated peptide. Right, quantification of binding. $^{***}p < 0.001$, one-way ANOVA, $n = 4$ cultures/group.

(F) Representative traces showing the inhibition of the mmu-miR-711-induced inward currents by the blocking peptide but not the mutated peptide (25 μ M) in hTRPA1-expressing HEK293 cells.

(G) Quantification of the inward currents in (F). $^{***}p < 0.001$, $^{**}p < 0.01$ versus vehicle, one-way ANOVA, $n = 5$ –10 cells/group.

(H) The blocking peptide (2 mM, 15 μ L) inhibits pruritus in mice induced by intradermal injection of mmu-miR-711 (1 mM, 10 μ L) but has no effects on pruritus evoked by chloroquine (CQ, 100 μ g/10 μ L) and compound 48/80 (48/80, 50 μ g/10 μ L). $^{**}p < 0.01$, $^{***}p < 0.001$, one-way ANOVA, $n = 5$ mice/group.

Data are represented as mean \pm SEM. See also Figure S6.

currents and pruritus (Figures 6E–6H). Taken together, our data demonstrate that the miR-711/TRPA1 interaction is critically involved in pruritus by miR-711.

A Mouse Model of CTCL Exhibits Chronic Itch and miRNA Dysregulation

To further address the physiological and pathological relevance of miR-711 in chronic itch, we developed a murine xenograft model of chronic itch to recapitulate human symptoms of cutaneous T cell lymphoma (CTCL), using Myla cell line (CD4⁺ memory T cells) from a CTCL patient (Ralfkiaer et al., 2011). Intra-

dermal inoculation of Myla cells induced profound lymphoma on the back skin of immune-deficient scid mice, with a slow but persistent tumor growth; tumor was evident on day 15 and continued to grow on day 40 (Figures 7A–7C and S7). Strikingly, this CTCL model was also characterized by an early onset of itch, prior to the onset of tumor growth: scratching behavior began on day 5 and reached to a peak on day 15 (Figure 7D). This early onset of pruritus may result from pruritogen(s) secreted from the inoculated human cells. Notably, pruritus declined from the peak on day 25 and day 30 but returned to the peak level on Day 40 (Figure 7D), suggesting a development of chronic itch.

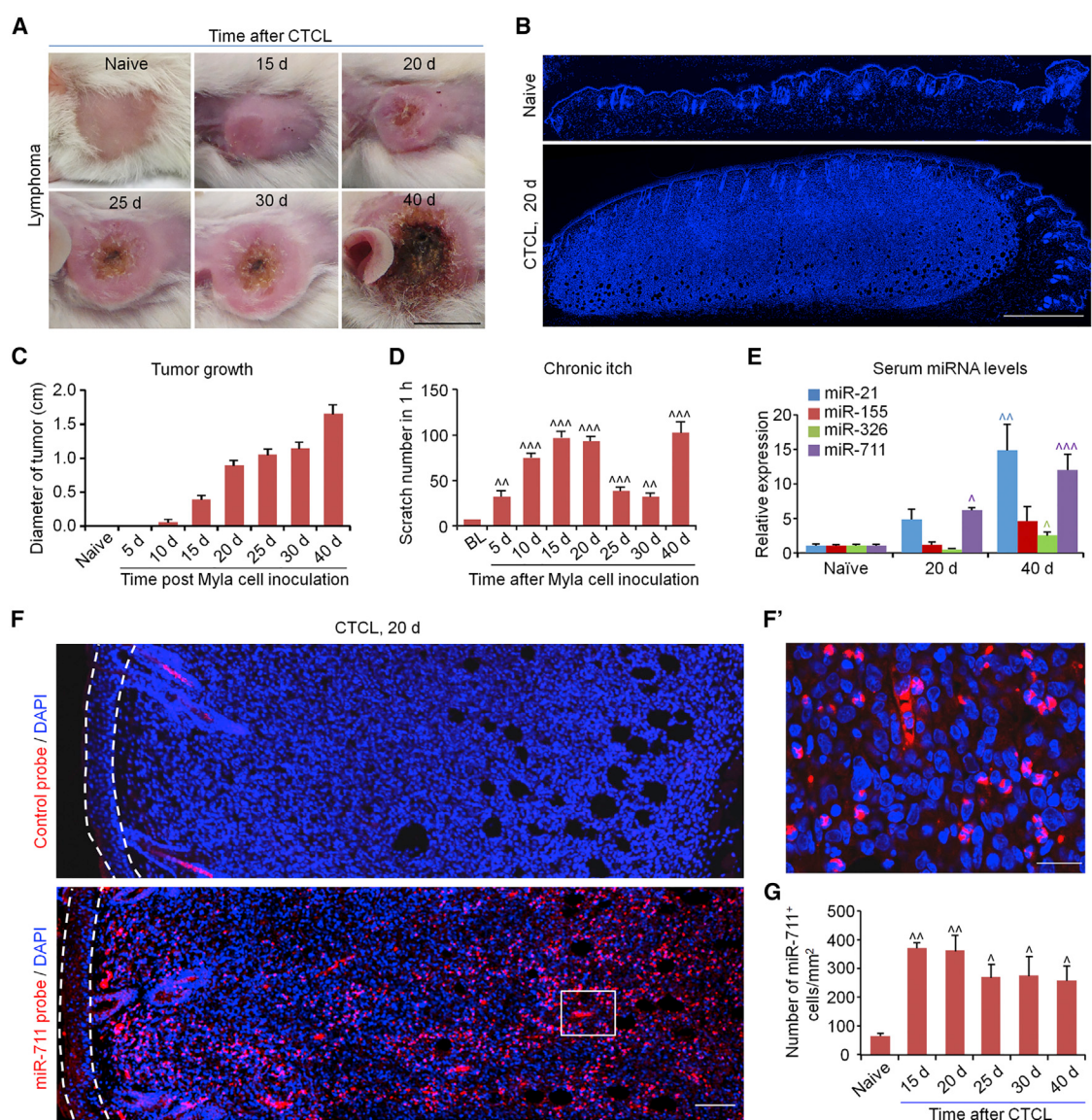


Figure 7. A Mouse Model of CTCL Showing Chronic Itch and miR-711 Upregulation

(A) Images of lymphomas on back skins at 15, 20, 25, 30, and 40 days after inoculation by intradermal injection of CD4⁺ Myla cells (1×10^5 cells/ μ L, 100 μ L). Scale, 10 mm.

(B) Images of DAPI staining of normal and tumor-bearing skins after CTCL. Scale, 1 mm.

(C) Time course of tumor growth, revealed by diameters of tumors after inoculation of CD4⁺ Myla cells.

(D) Time course of CTCL-evoked chronic itch. Number of scratches in 1 hr was counted blindly from the recorded videos. $^{^\wedge}p < 0.01$, $^{^\wedge\wedge}p < 0.001$, one-way ANOVA, versus baseline (BL), n = 6–9 mice/group.

(E) Relative serum levels of hsa-miR-21, hsa-miR-155, hsa-miR-326, and hsa-miR-711 of naive and CTCL mice. $^{\wedge}p < 0.05$, $^{^\wedge}p < 0.01$, versus respective naive mice, one-way ANOVA, n = 3–4 mice/group.

(F) In situ hybridization (red) showing hsa-miR-711 expression in lymphoma cells on the back skin 20 days after CTCL induction. The skin sections were counter-stained with DAPI (blue) to label nuclei. Note no signal is detected by the control probe. Scale, 100 μ m.

(F') Enlarged box in (F) showing single and double staining. Scale, 25 μ m.

(G) Quantification of hsa-miR-711-positive cells per square mm back skin at different times of CTCL. $^{\wedge}p < 0.05$, $^{^\wedge}p < 0.01$, versus naive control, one-way ANOVA, n = 4 mice/group.

Data are represented as mean \pm SEM. See also Figure S7.

Mouse CTCL was also associated with increases in the thickness of epidermis (hypertrophy) and dermis with lymphoma progress (Figure S7).

In parallel with dysregulations of miR-21, miR-155, miR-326, and miR-711 in CTCL patients (Ralfkiaer et al., 2011; Sandoval et al., 2015), we found increased levels of hsa-miR-21,

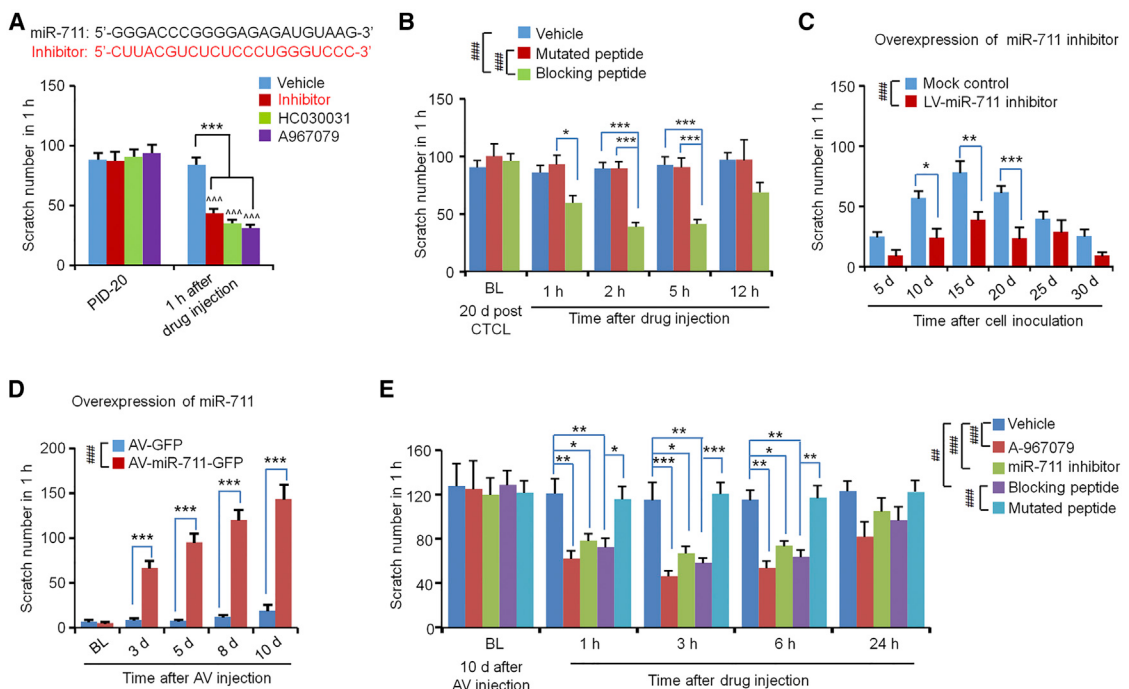


Figure 8. Inhibition of Chronic Itch by miR-711 Inhibitor, TRPA1 Antagonists, and miR-711/TRPA1 Interaction Blocking Peptide in a Mouse Model of CTCL

(A) Inhibition of CTCL-evoked chronic itch by intradermal injection of hsa-miR-711 inhibitor (100 μ M with a complementary sequence to hsa-miR-711) and TRPA1 antagonists (200 μ M HC030031 and 50 μ M A967069), 20 days after CD4 $^{+}$ Myla cell inoculation. ***p < 0.001, ^AAp < 0.001, versus vehicle, one-way ANOVA, n = 6 mice/group.

(B) Inhibition of CTCL-evoked chronic itch by the blocking peptide (2 mM), given 20 days after the Myla cell inoculation. *p < 0.05, ***p < 0.001, ***#p < 0.001, two-way ANOVA, n = 6–7 mice/group. BL, baseline.

(C) Overexpression of hsa-miR-711 inhibitor in Myla cells via lentivirus (LV) before the inoculation attenuates chronic itch after CTCL. *p < 0.05, **p < 0.01, ***p < 0.001, versus Mock control, ##p < 0.001, two-way ANOVA, n = 5–7 mice/group.

(D) Overexpression of hsa-miR-711 via adenovirus (AV, 10 μ L, titer of 2×10^{11} GC/ μ L) induces persistent itch after intradermal AV injection on the back skin. ***p < 0.001, versus control AV-GFP, ##p < 0.001, versus control AV-GFP, two-way ANOVA, n = 6 mice/group.

(E) Inhibition of hsa-miR-711 AV-induced persistent itch by intradermal injection of A-967079 (50 μ M), hsa-miR-711 inhibitor (100 μ M), and the blocking peptide (2 mM) 10 days after the AV injection. *p < 0.05, **p < 0.01, ***p < 0.001, ##p < 0.01, ***#p < 0.001, two-way ANOVA, n = 5–6 mice/group.

Data are represented as mean \pm SEM. See also Figures S7 and S8.

hsa-miR-155, hsa-miR-326, and hsa-miR-711 (Figure 7E) in mouse serum, 20 and 40 days after murine CTCL. Since these are human miRNAs, they must be derived from inoculated human lymphoma cells. *In situ* hybridization demonstrated a persistent and broad expression of hsa-miR-711 in the back skin of CTCL mice (Figures 7F and 7G). High levels of hsa-miR-711 were also detected in the culture medium of Myla cells (\approx 200 million copies per microliter) and Hut102 cells from another human lymphoma cell line, but not mouse B16 melanoma cells (Figures S8A and S8B), further suggesting that hsa-miR-711 can be secreted from human lymphoma cells. Notably, mouse- and human-derived miR-711, mmu-miR-711, and hsa-miR-711 differ in two nucleotides but share the same core sequence (Figure 1C). qPCR analysis detected high copy numbers of hsa-miR-711 but very low copy numbers of mmu-miR-711 in serum samples of CTCL mice, and a similar result was obtained when the data were plotted as Ct values (Figures S8C and S8D). These data suggest that (1) qPCR is highly specific to distinguish human versus mouse miR-711 and (2) miR-711 in mouse serum is predominantly derived from inoculated

human lymphoma cells. Strikingly, skin lymphoma was innervated by skin nerve fibers labeled with PGP-9.5 (Figure S8E). Thus, tumor-released miR-711 could trigger pruritus by activating adjacent nerve fibers which express TRPA1. These itch-inducing nerve fibers could be present in the tumor or nearby epidermis.

miR-711 Regulates Chronic Itch after CTCL

To determine a role of miR-711 in chronic itch, we employed several pharmacological and genetic approaches to target miR-711. First, intratumoral injection of a miR-711 inhibitor with a complementary sequence to hsa-miR-711 (Figure 8A), given 20 days after Myla cell inoculation, reduced chronic pruritus (Figure 8A). Second, CTCL-induced chronic itch was suppressed by two structurally different TRPA1 antagonists, HC030031 and A967069 (Figure 8A). Third, disruption of the miR-711 and TRPA1 interaction with the blocking peptide but not mutated peptide, given 20 days after the Myla cell inoculation, effectively reduced the CTCL-evoked chronic itch for more than 5 hr (Figure 8B). Fourth, to achieve a sustained

inhibition of miR-711, we generated a stable cell line expressing hsa-miR-711 inhibitor in Myla cells before the inoculation. Overexpression of the miR-711 inhibitor via lentivirus (LV) delayed the development of chronic itch for 20 days (Figure 8C), without affecting the tumor growth (Figure S8F). Fifth, overexpression of miR-711 via adenovirus (AV) resulted in persistent itch for more than 10 days and increased serum levels of hsa-miR-711 (Figures 8D and S8G), indicating that sustained miR-711 increase in serum is associated with chronic itch. Finally, we confirmed that chronic itch, evoked by miR-711 overexpression via AV, is mediated by miR-711, TRPA1, and the miR-711/TRPA1 interaction, because the AV-induced pruritus was suppressed by the miR-711 inhibitor, the TRPA1 antagonist, and the blocking peptide (Figure 8E). Taken together, these loss-of-function and gain-of-function experiments demonstrated that miR-711 is critically involved in chronic itch through TRPA1.

DISCUSSION

This study reveals an unconventional signaling role of miRNA and has conceptual advances in RNA biology. Intracellular miRNAs regulate gene expression post-transcriptionally, but extracellular miRNAs such as miR-let-7b are also present in culture medium and CSF of patients with Alzheimer's disease (Lehmann et al., 2012; Park et al., 2014). Especially, miR-let-7b exhibits biological roles by binding to TLR7 in sensory and cortical neurons via the GUUGUGU sequence, leading to neurodegeneration in cortical neurons (Lehmann et al., 2012) and neuronal excitation in nociceptive neurons (Park et al., 2014). In sharp contrast to previous studies, this study has revealed a TLR7-independent action of miRNA: extracellular miR-711 directly binds and activates TRPA1 on heterologous cells and primary sensory neurons. Therefore, extracellular miRNAs regulate neuronal function via both TLR7-dependent and TLR7-independent mechanisms. Interestingly, miRNA-711 and miR-let-7b induce distinct sensory responses, pruritus in this study but nociception in the previous study (Park et al., 2014).

One of the most striking findings of this study is to demonstrate direct interaction between miRNA (miR-711) and ion channel (TRPA1). Binding assays revealed that miR-711 but not mutant miRNA binds TRPA1 in HEK293 cells and mouse DRG neurons via the GGGACCC core sequence. Patch-clamp recordings showed that miR-711 is sufficient to induce TRPA1 currents in HEK293 cells and native DRG neurons via the core sequence. Single channel recordings indicated an interaction of miR-711 and TRPA1 on the cell surface. Typical TRPA1 agonists are pungent natural compounds and environmental irritants that covalently bind cysteine residues at the intracellular C-terminal (Macpherson et al., 2007). Through computer simulation, mutagenesis analysis, and electrophysiology validation, we identified several unknown extracellular sites of TRPA1 that interact with miR-711 core sequence (GGGACCC). This core sequence is sufficient to activate TRPA1 and binds multiple residues at the extracellular loops of mTRPA1 including residue P937 (equivalent to P934 of hTRPA1) in the S5-S6 loop. Mutation of P937 blocks the TRPA1-mediated inward current, induced by miR-711 but not by AITC. Thus, we have revealed unique TRPA1 activation sites by miRNA. The extracellular binding of

miR-711 is also supported by distinct responses in outside-out and inside-out single-channel recordings following miR-711 stimulation (Figures 2H–2K). Since individual oligonucleotides A, U, C, and G did not activate TRPA1 and produce pruritus (data not shown), TRPA1 binding by multiple nucleotides may be necessary.

This study has provided new insights into sensory neurobiology of pain and itch. Most pruritogens such as histamine, serotonin, endothelin, PAR2 agonist, and imiquimod also induce pain at high doses (Liu et al., 2010; Ma, 2010). AITC was regarded as an algogen (Ross, 2011). We found in the cheek model that intradermal AITC also evoked itch in a dose-dependent manner: only itch at low concentrations, both itch and pain at medium concentrations, only pain at the highest concentration (Figure S1A). This U-shape response of itch and pain may support the intensity theory, which states that a strong activation of nociceptive/pruriceptive sensory neurons elicits pain, whereas a weak activation of these sensory neurons induces itch (LaMotte et al., 2014; McMahon and Koltzenburg, 1992). This study also supports “labeled line” and “specificity” theory of itch (LaMotte et al., 2014). We identified miR-711 as a previously unknown itch mediator or pruritogen. Thus, intradermal miR-711 evoked itch but not pain even at the highest we tested. Indeed, miR-711 is a potent pruritogen and caused skin lesion at high dose (Figure S1B). Our calcium imaging suggests that miR-711 activates a subset of TRPA1 population (4% DRG neurons by miR-711 versus 23% DRG neurons by AITC). Because miR-711-responding neurons also showed responses to CQ and histamine (Figure 3), they may serve as a specific population of pruriceptors. It remains to be investigated whether this subset of TRPA1 neurons has high expression of TRPA1. It is also possible that this subpopulation has high surface expression of TRPA1, given the fact miR-711 activates the channel from the extracellular site, in contrast to intracellular activation of TRPA1 by AITC. Together, our findings are in agreement with both hypotheses of itch: “intensity coding” and “labeled line coding.”

TRPA1 mediates both pain and itch. How could activation of the same receptor trigger such different sensory responses? We postulate that rapid and transient activation of TRPA1 from the extracellular side (presumably in a subset of TRPA1⁺ neurons) by miR-711 causes itch, whereas slow and persistent activation of TRPA1 from the intracellular side by AITC results in pain. Compared to AITC (Bobkov et al., 2011; Karashima et al., 2010), miR-711 caused less increase in calcium permeability and evoked a weaker calcium response. It is noteworthy that it requires a low concentration of miR-711 (10 μM) to trigger inward currents and action potentials but a high concentration (50 μM) to evoke calcium responses in mouse DRG neurons. Unlike AITC, intraplantar injection miR-711 does not induce neurogenic inflammation in hindpaw. miR-711 also elicited a faster action potential than AITC with a shorter latency. These differences in TRPA1 activation may underlie distinct sensory behaviors (itch versus pain). In future studies, we will identify distinct neurotransmitters and neurocircuits involved in distinct activation of TRPA1 by miR-711 and AITC, leading to distinct pain and itch response.

Chronic pruritus is characteristic of several dermatologic diseases (e.g., atopic eczema, psoriasis) (Yosipovitch and

Bernhard, 2013). CTCLs are the most frequent primary skin lymphomas (Ralfkiaer et al., 2011). Patients with CTCL suffer from debilitating pruritus, but there is no standardized approach to treating pruritus in CTCL (Field et al., 2016). We developed a new mouse model of CTCL, showing remarkable chronic itch, associated with upregulations of circulating miRNAs (hsa-miR-21, hsa-miR-155, hsa-miR-326, and hsa-miR-711) in mouse serum. These miRNAs are also induced in CTCL patients (Ralfkiaer et al., 2011). Among these dysregulated miRNAs, only miR-711 induces itch. Furthermore, persistent expression of exogenous miR-711 on back skin via a viral vector is sufficient to drive chronic itch. Importantly, we demonstrate that extracellular miRNAs have physiological relevance and are drug targets for disease modification. Targeting extracellular miR-711 using a specific inhibitor with a complementary sequence or disrupting the miR-711/TRPA1 interaction with a blocking peptide each effectively alleviated chronic itch after CTCL. Given the broad expression of TRPA1 in various tissues, the blocking peptide may produce fewer side effects than a general TRPA1 blocker.

STAR★METHODS

Detailed methods are provided in the online version of this paper and include the following:

- KEY RESOURCES TABLE
- CONTACT FOR REAGENT AND RESOURCE SHARING
- EXPERIMENTAL MODEL AND SUBJECT DETAILS
 - Animals
 - Mouse CTCL Xenograft Model of Chronic Itch
 - Mouse DRG cultures
 - Human DRGs
- METHOD DETAILS
 - Constructs
 - Behavioral Assessment for Scratching (Itch) and Wiping (Pain)
 - Pain Tests for Mechanical and Thermal Sensitivity
 - Evans Blue Extravasation
 - Cell Culture and Transfection
 - Generation of Myla Stable Cell Line Expressing miR-711 Inhibitor
 - Primary Cultures of Mouse and Human Sensory Neurons
 - Whole-Cell Patch Clamp Recordings in HEK293 Cells, CHO Cells, and DRG Neurons
 - Inside-Out and Outside-Out Patch Clamp Recordings on HEK293 Cells
 - Ca²⁺ Imaging
 - Live Cell Labeling and Immunocytochemistry in Mouse DRG Neurons
 - RNA Pull-Down Assay and Immunoblotting
 - Fluorescent *In Situ* Hybridization (FISH)
 - miRNA Measurement by Quantitative Real-Time RT-PCR (qPCR)
 - Computer Simulations
- QUANTIFICATION AND STATISTICAL ANALYSIS
- DATA AND SOFTWARE AVAILABILITY

SUPPLEMENTAL INFORMATION

Supplemental information includes eight figures and one table and can be found with this article online at <https://doi.org/10.1016/j.neuron.2018.06.039>.

ACKNOWLEDGMENTS

This study is supported by NIH R01 grants NS87988, DE17794, and DE22743 to R.-R.J., and NIH grants R01GM11401 and R01GM064803 to N.V.D.

AUTHOR CONTRIBUTIONS

Q.H. developed the project, designed the mutations and blocking peptide, and performed behavioral and biochemical experiments; D.L. conducted electrophysiology in heterologous cells and DRG neurons; M.C. and N.V.D. conducted computer simulations and modeling of the miR-711/TRPA1 interaction; Z.W., C.J., and Y.H.K. conducted calcium imaging and electrophysiology experiments; X.L. measured miRNA secretion; X.Z. and A.N. contributed to calcium imaging. R.-R.J. supervised the project; R.-R.J., Q.H., M.C., and N.V.D. wrote the paper.

DECLARATION OF INTERESTS

The authors declare no competing interests.

Received: January 8, 2018

Revised: April 4, 2018

Accepted: June 25, 2018

Published: July 19, 2018

REFERENCES

- Alemi, F., Kwon, E., Poole, D.P., Lieu, T., Lyo, V., Cattaruzza, F., Cevikbas, F., Steinhoff, M., Nassini, R., Materazzi, S., et al. (2013). The TGR5 receptor mediates bile acid-induced itch and analgesia. *J. Clin. Invest.* **123**, 1513–1530.
- Anderson, M., Zheng, Q., and Dong, X. (2018). Investigation of pain mechanisms by calcium imaging approaches. *Neurosci. Bull.* **34**, 194–199.
- Andrade, A., Denome, S., Jiang, Y.Q., Marangoudakis, S., and Lipscombe, D. (2010). Opioid inhibition of N-type Ca²⁺ channels and spinal analgesia couple to alternative splicing. *Nat. Neurosci.* **13**, 1249–1256.
- Bartel, D.P. (2004). MicroRNAs: genomics, biogenesis, mechanism, and function. *Cell* **116**, 281–297.
- Bautista, D.M., Jordt, S.E., Nikai, T., Tsuruda, P.R., Read, A.J., Poblete, J., Yamoah, E.N., Basbaum, A.I., and Julius, D. (2006). TRPA1 mediates the inflammatory actions of environmental irritants and proalgesic agents. *Cell* **124**, 1269–1282.
- Bobkov, Y.V., Corey, E.A., and Ache, B.W. (2011). The pore properties of human nociceptor channel TRPA1 evaluated in single channel recordings. *Biochim. Biophys. Acta* **1808**, 1120–1128.
- Bourane, S., Duan, B., Koch, S.C., Dalet, A., Britz, O., Garcia-Campmany, L., Kim, E., Cheng, L., Ghosh, A., Ma, Q., and Goulding, M. (2015). Gate control of mechanical itch by a subpopulation of spinal cord interneurons. *Science* **350**, 550–554.
- Bradford, P.T., Devesa, S.S., Anderson, W.F., and Toro, J.R. (2009). Cutaneous lymphoma incidence patterns in the United States: a population-based study of 3884 cases. *Blood* **113**, 5064–5073.
- Chang, W., Berta, T., Kim, Y.H., Lee, S., Lee, S.Y., and Ji, R.R. (2018). Expression and role of voltage-gated sodium channels in human dorsal root ganglion neurons with special focus on Nav1.7, species differences, and regulation by paclitaxel. *Neurosci. Bull.* **34**, 4–12.
- Chen, X., Ba, Y., Ma, L., Cai, X., Yin, Y., Wang, K., Guo, J., Zhang, Y., Chen, J., Guo, X., et al. (2008). Characterization of microRNAs in serum: a novel class of biomarkers for diagnosis of cancer and other diseases. *Cell Res.* **18**, 997–1006.

- Dixon, W.J. (1980). Efficient analysis of experimental observations. *Annu. Rev. Pharmacol. Toxicol.* 20, 441–462.
- Dokholyan, N.V., Buldyrev, S.V., Stanley, H.E., and Shakhnovich, E.I. (1998). Discrete molecular dynamics studies of the folding of a protein-like model. *Fold. Des.* 3, 577–587.
- Field, H., Gao, L., Matwani, P., and Wong, H.K. (2016). Pruritus reduction with systemic anti-lymphoma treatments in patients with cutaneous T cell lymphoma: a narrative review. *Dermatol. Ther.* (Heidelb.) 6, 579–595.
- Han, L., Ma, C., Liu, Q., Weng, H.J., Cui, Y., Tang, Z., Kim, Y., Nie, H., Qu, L., Patel, K.N., et al. (2013). A subpopulation of nociceptors specifically linked to itch. *Nat. Neurosci.* 16, 174–182.
- Han, Q., Kim, Y.H., Wang, X., Liu, D., Zhang, Z.J., Bey, A.L., Lay, M., Chang, W., Berta, T., Zhang, Y., et al. (2016). SHANK3 deficiency impairs heat hyperalgesia and TRPV1 signaling in primary sensory neurons. *Neuron* 92, 1279–1293.
- Hargreaves, K., Dubner, R., Brown, F., Flores, C., and Joris, J. (1988). A new and sensitive method for measuring thermal nociception in cutaneous hyperalgesia. *Pain* 32, 77–88.
- Huang, J., Polgar, E., Solinski, H.J., Mishra, S.K., Tseng, P.Y., Iwagaki, N., Boyle, K.A., Dickie, A.C., Kriegbaum, M.C., Wildner, H., et al. (2018). Circuit dissection of the role of somatostatin in itch and pain. *Nat. Neurosci.* 21, 707–716.
- Ji, R.R. (2018). Recent progress in understanding the mechanisms of pain and itch: the second special issue. *Neurosci. Bull.* 34, 1–3.
- Ji, R.R., Xu, Z.Z., and Gao, Y.J. (2014). Emerging targets in neuroinflammation-driven chronic pain. *Nat. Rev. Drug Discov.* 13, 533–548.
- Karashima, Y., Preneen, J., Talavera, K., Janssens, A., Voets, T., and Nilius, B. (2010). Agonist-induced changes in Ca(2+) permeation through the nociceptor channel TRPA1. *Biophys. J.* 98, 773–783.
- Kardon, A.P., Polgár, E., Hachisuka, J., Snyder, L.M., Cameron, D., Savage, S., Cai, X., Karnup, S., Fan, C.R., Hemenway, G.M., et al. (2014). Dynorphin acts as a neuromodulator to inhibit itch in the dorsal horn of the spinal cord. *Neuron* 82, 573–586.
- Kittaka, H., Uchida, K., Fukuta, N., and Tominaga, M. (2017). Lysophosphatidic acid-induced itch is mediated by signalling of LPA₅ receptor, phospholipase D and TRPA1/TRPV1. *J. Physiol.* 595, 2681–2698.
- Kota, P., Ding, F., Ramachandran, S., and Dokholyan, N.V. (2011). Gaia: automated quality assessment of protein structure models. *Bioinformatics* 27, 2209–2215.
- Krokhutin, A., Houlihan, K., and Dokholyan, N.V. (2015). iFoldRNA v2: folding RNA with constraints. *Bioinformatics* 31, 2891–2893.
- LaMotte, R.H., Dong, X., and Ringkamp, M. (2014). Sensory neurons and circuits mediating itch. *Nat. Rev. Neurosci.* 15, 19–31.
- Lehmann, S.M., Krüger, C., Park, B., Derkow, K., Rosenberger, K., Baumgart, J., Trimbuch, T., Eom, G., Hinz, M., Kaul, D., et al. (2012). An unconventional role for miRNA: let-7 activates Toll-like receptor 7 and causes neurodegeneration. *Nat. Neurosci.* 15, 827–835.
- Liu, Q., Tang, Z., Surdenikova, L., Kim, S., Patel, K.N., Kim, A., Ru, F., Guan, Y., Weng, H.J., Geng, Y., et al. (2009). Sensory neuron-specific GPCR Mrgprs are itch receptors mediating chloroquine-induced pruritus. *Cell* 139, 1353–1365.
- Liu, T., Xu, Z.Z., Park, C.K., Berta, T., and Ji, R.R. (2010). Toll-like receptor 7 mediates pruritus. *Nat. Neurosci.* 13, 1460–1462.
- Liu, B., Escalera, J., Balakrishna, S., Fan, L., Caceres, A.I., Robinson, E., Sui, A., McKay, M.C., McAlexander, M.A., Herrick, C.A., and Jordt, S.E. (2013). TRPA1 controls inflammation and pruritogen responses in allergic contact dermatitis. *FASEB J.* 27, 3549–3563.
- Liu, T., Han, Q., Chen, G., Huang, Y., Zhao, L.X., Berta, T., Gao, Y.J., and Ji, R.R. (2016). Toll-like receptor 4 contributes to chronic itch, allodynia, and spinal astrocyte activation in male mice. *Pain* 157, 806–817.
- Ma, Q. (2010). Labeled lines meet and talk: population coding of somatic sensations. *J. Clin. Invest.* 120, 3773–3778.
- Macpherson, L.J., Dubin, A.E., Evans, M.J., Marr, F., Schultz, P.G., Cravatt, B.F., and Patapoutian, A. (2007). Noxious compounds activate TRPA1 ion channels through covalent modification of cysteines. *Nature* 445, 541–545.
- McMahon, S.B., and Koltzenburg, M. (1992). Itching for an explanation. *Trends Neurosci.* 15, 497–501.
- Meixiong, J., and Dong, X. (2017). Mas-related G protein-coupled receptors and the biology of itch sensation. *Annu. Rev. Genet.* 51, 103–121.
- Mishra, S.K., and Hoon, M.A. (2013). The cells and circuitry for itch responses in mice. *Science* 340, 968–971.
- Morita, T., McClain, S.P., Batia, L.M., Pellegrino, M., Wilson, S.R., Kienzler, M.A., Lyman, K., Olsen, A.S., Wong, J.F., Stucky, C.L., et al. (2015). HTR7 mediates serotonergic acute and chronic itch. *Neuron* 87, 124–138.
- Park, C.K., Xu, Z.Z., Berta, T., Han, Q., Chen, G., Liu, X.J., and Ji, R.R. (2014). Extracellular microRNAs activate nociceptor neurons to elicit pain via TLR7 and TRPA1. *Neuron* 82, 47–54.
- Patapoutian, A., Tate, S., and Woolf, C.J. (2009). Transient receptor potential channels: targeting pain at the source. *Nat. Rev. Drug Discov.* 8, 55–68.
- Paulsen, C.E., Armache, J.P., Gao, Y., Cheng, Y., and Julius, D. (2015). Structure of the TRPA1 ion channel suggests regulatory mechanisms. *Nature* 520, 511–517.
- Qureshi, R.A., Tian, Y., McDonald, M.K., Capasso, K.E., Douglas, S.R., Gao, R., Orlova, I.A., Barrett, J.E., Ajit, S.K., and Sacan, A. (2016). Circulating microRNA signatures in rodent models of pain. *Mol. Neurobiol.* 53, 3416–3427.
- Ralfkjaer, U., Hagedorn, P.H., Bangsgaard, N., Lovendorf, M.B., Ahler, C.B., Svensson, L., Kopp, K.L., Vennegaard, M.T., Lauenborg, B., Zibert, J.R., et al. (2011). Diagnostic microRNA profiling in cutaneous T-cell lymphoma (CTCL). *Blood* 118, 5891–5900.
- Roberson, D.P., Gudes, S., Sprague, J.M., Patoski, H.A., Robson, V.K., Blas, F., Duan, B., Oh, S.B., Bean, B.P., Ma, Q., et al. (2013). Activity-dependent silencing reveals functionally distinct itch-generating sensory neurons. *Nat. Neurosci.* 16, 910–918.
- Ross, S.E. (2011). Pain and itch: insights into the neural circuits of aversive somatosensation in health and disease. *Curr. Opin. Neurobiol.* 21, 880–887.
- Ross, S.E., Mardinly, A.R., McCord, A.E., Zurawski, J., Cohen, S., Jung, C., Hu, L., Mok, S.I., Shah, A., Savner, E.M., et al. (2010). Loss of inhibitory interneurons in the dorsal spinal cord and elevated itch in Blhfb5 mutant mice. *Neuron* 65, 886–898.
- Sandoval, J., Díaz-Lagares, A., Salgado, R., Servitje, O., Climent, F., Ortiz-Romero, P.L., Pérez-Ferriols, A., García-Muret, M.P., Estrach, T., García, M., et al. (2015). MicroRNA expression profiling and DNA methylation signature for deregulated microRNA in cutaneous T-cell lymphoma. *J. Invest. Dermatol.* 135, 1128–1137.
- Sharma, S., Ding, F., Nie, H., Watson, D., Unnithan, A., Lopp, J., Pozefsky, D., and Dokholyan, N.V. (2006). iFold: a platform for interactive folding simulations of proteins. *Bioinformatics* 22, 2693–2694.
- Shimada, S.G., and LaMotte, R.H. (2008). Behavioral differentiation between itch and pain in mouse. *Pain* 139, 681–687.
- Shirvanyants, D., Ding, F., Tsao, D., Ramachandran, S., and Dokholyan, N.V. (2012). Discrete molecular dynamics: an efficient and versatile simulation method for fine protein characterization. *J. Phys. Chem. B* 116, 8375–8382.
- Story, G.M., Peier, A.M., Reeve, A.J., Eid, S.R., Mosbacher, J., Hricik, T.R., Earley, T.J., Hergarden, A.C., Andersson, D.A., Hwang, S.W., et al. (2003). ANKTM1, a TRP-like channel expressed in nociceptive neurons, is activated by cold temperatures. *Cell* 112, 819–829.
- Sun, Y.G., and Chen, Z.F. (2007). A gastrin-releasing peptide receptor mediates the itch sensation in the spinal cord. *Nature* 448, 700–703.
- Sun, Y.G., Zhao, Z.Q., Meng, X.L., Yin, J., Liu, X.Y., and Chen, Z.F. (2009). Cellular basis of itch sensation. *Science* 325, 1531–1534.
- Sun, S., Xu, Q., Guo, C., Guan, Y., Liu, Q., and Dong, X. (2017). Leaky gate model: intensity-dependent coding of pain and itch in the spinal cord. *Neuron* 93, 840–853.e5, e845.

- Wang, Y.Y., Chang, R.B., Waters, H.N., McKemy, D.D., and Liman, E.R. (2008). The nociceptor ion channel TRPA1 is potentiated and inactivated by permeating calcium ions. *J. Biol. Chem.* **283**, 32691–32703.
- Webb, B., and Sali, A. (2014). Protein structure modeling with MODELLER. *Methods Mol. Biol.* **1137**, 1–15.
- Wilson, S.R., Gerhold, K.A., Bifolck-Fisher, A., Liu, Q., Patel, K.N., Dong, X., and Bautista, D.M. (2011). TRPA1 is required for histamine-independent, Mas-related G protein-coupled receptor-mediated itch. *Nat. Neurosci.* **14**, 595–602.
- Wilson, S.R., Nelson, A.M., Batia, L., Morita, T., Estandian, D., Owens, D.M., Lumpkin, E.A., and Bautista, D.M. (2013a). The ion channel TRPA1 is required for chronic itch. *J. Neurosci.* **33**, 9283–9294.
- Wilson, S.R., Thé, L., Batia, L.M., Beattie, K., Katibah, G.E., McClain, S.P., Pellegrino, M., Estandian, D.M., and Bautista, D.M. (2013b). The epithelial cell-derived atopic dermatitis cytokine TSLP activates neurons to induce itch. *Cell* **155**, 285–295.
- Xu, Z.Z., Kim, Y.H., Bang, S., Zhang, Y., Berta, T., Wang, F., Oh, S.B., and Ji, R.R. (2015). Inhibition of mechanical allodynia in neuropathic pain by TLR5-mediated A-fiber blockade. *Nat. Med.* **21**, 1326–1331.
- Yosipovitch, G., and Bernhard, J.D. (2013). Clinical practice. chronic pruritus. *N. Engl. J. Med.* **368**, 1625–1634.
- Zhou, R., Berne, B.J., and Germain, R. (2001). The free energy landscape for beta hairpin folding in explicit water. *Proc. Natl. Acad. Sci. USA* **98**, 14931–14936.

STAR★METHODS

KEY RESOURCES TABLE

REAGENT or RESOURCE	SOURCE	IDENTIFIER
Antibodies		
Rabbit polyclonal Anti-TRPA1 (extracellular) antibody	Alomone Labs	RRID: AB_2040232
Bacterial and Virus Strains		
MISSION Lenti microRNA Inhibitor (hsa-miR-711) lentivirus	Sigma	Cat# HLTUD0996
Control GFP Adenovirus	Vigene Biosciences	Cat#CV10001
Premade Adenovirus for Human miR-711	Vigene Biosciences	Cat#VR233338
A967079	Sigma	Cat# SML0085
AITC	Sigma	Cat# W203408
Blocking peptide: NH ₂ -FRNELAYPVLTFGQL-COOH	Sigma	N/A
Mutated peptide: NH ₂ -FRNELAAAVATFGQL-COOH	Sigma	N/A
Critical Commercial Assays		
In-Fusion HD Cloning Kit	Takara Bio	Cat #121416
Q5 Site-Directed Mutagenesis Kit	New England Biolabs	Cat #E0554S
miRNeasy Serum/Plasma Kit	Qiagen	Cat #217184
miScript II RT Kit	Qiagen	Cat #218160
miScript miRNA assay for hsa-miR-711	Qiagen	Cat #MS00017325
miScript miRNA assay for hsa-miR-21	Qiagen	Cat #MS00009079
miScript miRNA assay hsa-miR-155	Qiagen	Cat #MS00031486
miScript miRNA assay hsa-miR-326	Qiagen	Cat #MS00003948
miScript miRNA assay mmu-miR-711	Qiagen	Cat #MS00002975
Experimental Models: Cell Lines		
HEK293-hTRPA1 stable cell line	SB Drug Discovery	SB-HEK-TRPA1
CD4 ⁺ Myla cell	Sigma	Cat#95051032
Experimental Models: Organisms/Strains		
Mouse:NOD.CB17- <i>Prkdc</i> ^{scid}	The Jackson Laboratory	JAX: 001303
Mouse:B6;129P- <i>Trpa1</i> ^{tm1Kykw}	The Jackson Laboratory	JAX: 006401
Oligonucleotides		
mmu-miR-711-bio: gggaccggggagagauguag-bio	Sigma	N/A
mmu-miR-711(m6)-bio: aaaaaaggggagagauguag-bio	Sigma	N/A
mmu-miR-711-cy3: gggaccggggagagauguag-cy3	Sigma	N/A
mmu-miR-711(m6)-cy3: aaaaaaggggagagauguag-cy3	Sigma	N/A
hsa-miR-711 inhibitor: cuuacgucucucccuggguccc	Shanghai GenePharm	N/A
(DIG)-labeled miRCURY LNA Detection probe against hsa-miR-711	Exiqon	Cat#612180-330
(DIG)-labeled miRCURY LNA Detection negative control	Exiqon	Cat# 699004-360
Recombinant DNA		
Plasmid: pcDNA3.1- <i>mTrpv1</i> , <i>mTrpv2</i> , <i>mTrpv3</i> , <i>mTrpv4</i>	Sun Work Hwang, Korea University	N/A
Software		
Gaia	Kota et al., 2011	http://redshift.med.unc.edu/chiron/login.php
iFoldRNA	Krokhutin et al., 2015; Sharma et al., 2006	N/A

Also see Table S1 for additional resources and reagents.

CONTACT FOR REAGENT AND RESOURCE SHARING

Further information and requests for resources and reagents should be directed to and will be fulfilled by the Lead Contact Ru-Rong Ji (ru-rong.ji@duke.edu).

EXPERIMENTAL MODEL AND SUBJECT DETAILS

Animals

We purchased knockout mice including *Trpa1*^{-/-} mice (Stock No: 006401), *Tlr7*^{-/-} mice (Stock No: 008380) and *Trpv1*^{-/-} mice (Stock No: 008336) from Jackson Laboratories. All the knockout mice have C57B/6 background and viable, showing no developmental defects. Immune deficient mice (NOD.CB17-Prkdc^{scid}, Stock No: 001303, 129 background) were also obtained from Jackson Laboratories and used for generating the lymphoma model. We also used Pirt-GCaMP3 mice (Anderson et al., 2018) for calcium imaging. These mice were provided by Dr. Xinzhong Dong of Johns Hopkins University and Andrea Nackley of Duke University. Adult male mice (8-12 weeks), including knockout mice and the same background control mice, as well as some CD1 mice, were used for behavioral studies. Mice were group-housed at Duke University animal facilities on a 12 hr light/12 hr dark cycle at 22°C ± 1°C with free access to food and water. No statistical method was used to predetermine sample size. No randomization was applied to the animal experiments. Sample sizes were chosen based on our previous studies on similar tests (Liu et al., 2016; Liu et al., 2010). All the animal procedures were approved by the Institutional Animal Care & Use Committee of Duke University. Animal experiments were conducted in accordance with the National Institutes of Health Guide for the Care and Use of Laboratory Animals.

Mouse CTCL Xenograft Model of Chronic Itch

We developed a murine xenograft model of cutaneous T cell lymphoma (CTCL) using immune-deficient mice (NOD.CB17-Prkdc^{scid}, 8-10 weeks old, male). CD4⁺ MyLa cell line was purchased from Sigma (Ca#95051032). The cell line was established from a plaque biopsy of an 82-year old male with mycosis fungoides stage II by inclusion of IL-2 and IL-4 in the culture medium. CTCL was generated via intradermal injection of CD4⁺ Myla cells (1 × 10⁵ cells/μL, 100 μL) on the nape of the neck. Tumor growth was assessed for 40 days by measurements of tumor diameters.

Mouse DRG cultures

DRGs were collected from young mice (4-6 weeks) of both sexes for primary cultures. These cultures were maintained for less than 3 days for electrophysiological studies.

Human DRGs

Non-diseased human DRGs were obtained from donors through National Disease Research Interchange (NDRI) with permission of exemption from the Duke University Institutional Review Board (IRB). Postmortem L3-L5 DRGs were dissected from 4 donors: 18-year-old male, 54-year-old male, 42-year-old female, and 39-year-old female.

METHOD DETAILS

Constructs

The cDNAs of mouse pcDNA3.1-*Trpa1*, pcDNA3.1-*Trpv1*, pcDNA3.1-*Trpv2*, pcDNA3.1-*Trpv3*, and pcDNA3.1-*Trpv4* were kindly provided Dr. Sun Work Hwang from Korea University. Mouse *Trpa1* cDNA was subcloned into pCGN-HA backbone (Addgene) using In-Fusion HD Cloning Kit (Clontech Laboratories, CA). Q5 Site-Directed Mutagenesis Kit was used to generate *mTrpa1* mutant (M1-M13) based on pCGN-*mTrpa1*. All primers were listed in “[KEY RESOURCES TABLE](#).”

Behavioral Assessment for Scratching (Itch) and Wiping (Pain)

Mice were shaved on the cheek or nape after a brief anesthesia with isoflurane. Before experiments, mice were habituated in small plastic chambers (14 × 18 × 12 cm) daily for two days. The room temperature and humidity remained stable for all the experiments. Mice were then briefly removed from the chamber and given an intradermal injection of miRNAs, AITC, histamine, chloroquine (CQ), compound 48/80 (48/80), or peptide with the concentration and volume indicated in the figure legends. After the injection, the number of scratches in 60 min was counted. A scratch was counted when a mouse lifted its hind paw to scratch the shaved region and returned the paw to the floor or to the mouth. A bout of wiping was defined as a continuous wiping movement with a forepaw directing at the area of the injection area (Shimada and LaMotte, 2008). Scratching and wiping behavior was videoed for 30 min or 60 min using Sony HDR-CX610 camera. The video was subsequently played back offline and the numbers of scratches and wipes were quantified in a blinded manner.

Pain Tests for Mechanical and Thermal Sensitivity

Mice were habituated to the environment for at least 2 days before the testing. All the behaviors were tested blindly. Inflammatory pain after intraplantar AITC (10 mM, 10 μL) or miR-711 (1 mM, 10 μL) was measured on hind paws. For testing mechanical sensitivity,

we confined mice in boxes ($14 \times 18 \times 12$ cm) placed on an elevated metal mesh floor and stimulated their hind paws with a series of von Frey hairs with logarithmically increasing stiffness (0.16–2.00 g, Stoelting), presented perpendicularly to the central plantar surface. We determined the 50% paw withdrawal threshold by Dixon's up-down method (Dixon, 1980). Thermal sensitivity was tested using Hargreaves radiant heat apparatus (Hargreaves et al., 1988) (IITC Life Science). For the radiant heat test, the basal paw withdrawal latency was adjusted to 10–15 s, with a cutoff of 25 s to prevent tissue damage.

Evans Blue Extravasation

To examine neurogenic inflammation in a hind paw (Han et al., 2016), mice were anesthetized with 5% isoflurane. Evans blue (50 mg/kg body weight) was given intravenously 10 min before neurogenic irritant application. Capsaicin (1 mM, 10 μ L), AITC (5 mM, 10 μ L), or miR-711 (1 mM, 10 μ L) were given by intraplantar injection, and 30 min later mice were sacrificed and plantar tissues were collected and weighted. Evans blue was extracted from the tissues by incubation in 400 μ L formamide at 37°C for 48 hr. Evans blue was quantified by measuring the optical density of the formamide extract at 620 nm. Absorbance was normalized to per gram of tissue weight.

Cell Culture and Transfection

CD4⁺ Myla cell line was cultured in RPMI 1640 media (GIBCO), supplemented with 2 mM Glutamine (GIBCO), 100 U/mL IL-2 (Sigma), 100 U/mL IL-4 (Sigma), and 10% human AB serum (Sigma). HuT 102 cell line was cultured in RPMI 1640 supplemented with pyruvate, HEPES, and 10% (v/v) fetal bovine serum (HyClone). HEK293-hTRPA1 stable cell line was cultured in MEM (GIBCO) containing 2 mM Glutamine, 4 μ g/mL Blasticidin, 10% FBS (v/v). B16 and CHO cells were cultured in high glucose (4.5 g/L) Dulbecco's Modified Eagle's Medium (GIBCO) containing 10% (v/v) fetal bovine serum (GIBCO). Culture media were supplemented with 50 units/mL of penicillin and 50 μ g/mL streptomycin, and cultures were maintained with 5% CO₂ in 37°C incubator. Transfection (2 μ g cDNA) was performed with LipofectamineTM 2000 Reagent (Invitrogen) at 80% confluence and the transfected cells were cultured in the same media for 48 hr before electrophysiological and biochemical studies.

Generation of Myla Stable Cell Line Expressing miR-711 Inhibitor

CD4⁺ Myla cells were plated at a density of 2×10^5 cells/mL in 2 mL culture media in 6-well plates. For each well, 20 μ L of the MISSION Lenti microRNA Inhibitor (hsa-miR-711) lentivirus (Sigma) with a titer of 2.6×10^7 Tu/mL were added. Cell mixtures were incubated at 37°C for 48 hr, washed with PBS three times, and re-suspended in fresh culture media, and 24 hr later, 1 μ g/mL puromycin was added to the cells to select stably transduced cell populations. We tried to grow and passage the cells as much as necessary (usually 3 days) and maintained selection pressure by keeping 1 μ g/mL puromycin in the medium. After 4 weeks, a large number of the cells were killed; the remaining cells retained the expression of the plasmid, which stably integrates into the genome of the targeted cells. These cells were used for inoculation to generate the CTCL model for testing the effects of miR-711 inhibitor on chronic itch and tumor growth.

Primary Cultures of Mouse and Human Sensory Neurons

DRGs or TGs were removed aseptically from mice (4–6 weeks) and incubated with collagenase (1.25 mg/mL, Roche)/dispase-II (2.4 units/mL, Roche) at 37°C for 90 min, then digested with 0.25% trypsin for 8 min at 37°C, followed by 0.25% trypsin inhibitor. Cells were mechanically dissociated with a flame polished Pasteur pipette in the presence of 0.05% DNase I (Sigma). DRG cells were plated on glass coverslips and grown in a neurobasal defined medium (with 2% B27 supplement, Invitrogen) with 5 μ M AraC and 5% CO₂ at 36.5°C. DRG neurons were grown for 24 hr before use.

Non-diseased human DRGs were obtained from donors through National Disease Research Interchange (NDRI) with permission of exemption from the Duke University Institutional Review Board (IRB). Postmortem L3–L5 DRGs were dissected from 4 donors and delivered in ice cold culture medium to the laboratory at Duke University within 24–72 hr of the donor's death. Upon the delivery, DRGs were rapidly dissected from nerve roots and minced in a calcium-free HBSS (GIBCO). Human DRG cultures were prepared as previously reported (Chang et al., 2018; Han et al., 2016). DRGs were digested at 37°C in a humidified CO₂ incubator for 120 min with collagenase Type II (Worthington, 290 units/mg, 12 mg/mL final concentration) and dispase II (Roche, 1 unit/mg, 20 mg/mL) in PBS with 10 mM HEPES, pH adjusted to 7.4 with NaOH. DRGs were mechanically dissociated using fire-polished pipettes, filtered through a 100 μ m nylon mesh and centrifuged (500 g for 5 min). The pellet was resuspended, plated on 0.5 mg/mL poly-D-lysine-coated glass coverslips, and grown in Neurobasal medium supplemented with 10% FBS, 2% B-27 supplement, and 1% penicillin/streptomycin. Whole-cell patch-clamp recordings in small (< 50 μ m) human DRG neurons were conducted at room temperature using patch pipettes with resistances of 3–4 M Ω .

Whole-Cell Patch Clamp Recordings in HEK293 Cells, CHO Cells, and DRG Neurons

Whole-cell patch clamp recordings were performed at room temperature using an Axopatch-200B amplifier (Axon Instruments) with a Digidata 1440B (Axon Instruments). In this study, we only examined small-diameter mouse DRG neurons (< 25 μ m) and small-diameter human DRG neurons (< 55 μ m). The patch pipettes were pulled from borosilicate capillaries (World Precision Instruments) using a P-97 Flaming/Brown micropipette puller (Sutter Instrument). Pipette resistance was 4–6 M Ω for whole-cell and outside-out recording. For inward current recordings in mouse and human DRG neurons, HEK293 cells, and CHO cells, the internal solution contains

(in mM): 140 CsCl, 10 EGTA, 10 HEPES, and 2 Mg-ATP, adjusted to pH 7.3 with CsOH. Whole cell recordings were performed in an extracellular solution that contains (in mM): 140 NaCl, 5 KCl, 2 MgCl₂, 10 HEPES, and 10 glucose, adjusted to pH 7.4 with NaOH and osmolarity to 300–310 mOsm. To record miR-711 and AITC evoked action potentials, the amplifier was switched to the current-clamp mode. Action potential recordings were performed in small-diameter DRG neurons, with the following solutions: i) internal pipette solution contains: 126 mM K-gluconate, 10 mM NaCl, 1 mM MgCl₂, 10 mM EGTA, 10 mM HEPES and 2 mM Na-ATP, adjusted to pH 7.4 with KOH and osmolarity to 295–300 mOsm, and ii) extracellular solution contains: 140 mM NaCl, 5 mM KCl, 2 mM MgCl₂, 2 mM CaCl₂, 10 mM HEPES, 10 mM glucose, adjusted to pH 7.4 with KOH.

Calcium and sodium ion permeability experiments were conducted to compare the effects of miR-711 and AITC (Wang et al., 2008). Inward current recordings were made in TRPA1-expressing HEK293 cells with an Axopatch 200B amplifier and digitized with a Digidata 1440A digitizer, acquired with Clampex 10.6, and analyzed with Clampfit 10.6 (Axon Instruments, Union City, CA). Data were sampled at 10 kHz, and filtered at 2 kHz. The resistance of the pipettes was 4–5 MΩ. For measurement of ion permeability, the membrane potential was ramped from +80 mV to –80 mV (1 V/s). The recording solutions for ion permeability experiments are, i) bath solution: 145 mM NaCl, 10 mM HEPES, and 2 mM EDTA, or 128 mM CaCl₂ with 10 mM HEPES (pH 7.4 with NaOH), and ii) pipette solution: 145 mM CsCl, 2 mM MgATP, 10 mM HEPES (pH 7.4 with CsOH). The I/V curve and reversal potential were analyzed as previously demonstrated (Wang et al., 2008).

To test the effects of miR-711 on calcium channels, calcium currents were recorded in mouse DRG neurons (Andrade et al., 2010). Calcium current was evoked by a 40-ms step depolarization to –10 mV from the holding potential of –80 mV, using i) external solution (mM): 135 mM TEA-Cl, 1 mM CaCl₂, 10 mM HEPES, 4 mM MgCl₂ and 0.1 μM TTX, adjusted to a pH of 7.4 with TEA-OH, and ii) the pipette solution: 126 mM CsCl, 5 mM Mg-ATP, 10 mM EGTA and 10 mM HEPES, adjusted to a pH of 7.3 with CsOH.

Inside-Out and Outside-Out Patch Clamp Recordings on HEK293 Cells

For inside-out recordings in TRPA1-expressing HEK293 cells, pipette resistance was 8–10 MΩ and, the internal solution contains: 126 mM K-gluconate, 10 mM NaCl, 1 mM MgCl₂, 10 mM EGTA, 10 mM HEPES, and 2 Na-ATP (adjusted to pH 7.3 with KOH, osmolarity to 295–300 mOsm). The recordings were performed at room temperature in a bath solution (intracellular side) of 140 mM NaCl, 10 mM EGTA, 5 mM KCl, 2 mM CaCl₂, 1 mM MgCl₂, 10 mM HEPES, 10 mM glucose, adjusted to pH 7.4 with NaOH and osmolarity to 300–310 mOsm (Park et al., 2014). For comparison, outside-out recordings were also performed in TRPA1-expressing HEK293 cells in an extracellular solution of 140 mM NaCl, 5 mM KCl, 2 mM MgCl₂, 10 mM HEPES, and 10 mM glucose (adjusted to pH 7.4 with NaOH and osmolarity to 300–310 mOsm). The internal solution contains 140 mM CsCl, 10 mM EGTA, 10 mM HEPES, and 2 mM Mg-ATP, adjusted to pH 7.3 with CsOH. Currents were low-pass filtered at 2 kHz and digitized at a sampling rate of 10 kHz with Digidata-1440A (Axon Instruments). The pClamp10 (Axon Instruments) software was used during experiments and data analysis. Opening and closing transitions of single channels were detected by using 50% of the threshold criterion. All events were carefully checked before the analysis. When superimposed openings were observed, the number of channels in the patch was estimated from the maximal number of superimposed openings. The single-channel open probability (Po) was determined using the following equation: Po = T'/T, where T' is the total open time for a patch over time T.

Ca²⁺ Imaging

Ca²⁺ imaging was conducted in mouse DRG and TG neurons from Pirt-GCaMP3 mice (Anderson et al., 2018) at room temperature. The imaging buffer includes 140 mM NaCl, 10 mM D-(+)-Glucose, 1 mM MgCl₂, 2 mM CaCl₂, 5 mM KCl, 10 mM HEPES, pH = 7.4, osmolarity = 320 mOsm/L. Calcium signals were measured using green emitted light in a 3 s interval. Ca²⁺ signal amplitudes were presented as ΔF/F₀ = (F_t–F₀)/F₀ as ratio of fluorescence difference (F_t–F₀) to basal value (F₀). The average fluorescence intensity in the baseline period was taken as F₀. Ca²⁺ imaging was also analyzed in HEK293-TRPA1 cell line after loading cells with 2 μM fura2-AM (Invitrogen) for 40 min in the Ca²⁺ imaging buffer. Ca²⁺ imaging protocol was a ratio metric method with 340/380-nm wavelength light for dual excitation. Data were presented as ΔR/R₀, determined as the fraction ΔR (R_t–R₀) of the increase of a given ratio over baseline ratio (R₀).

Live Cell Labeling and Immunocytochemistry in Mouse DRG Neurons

Disassociated DRG neurons were plated on Poly-D-Lysine coated coverslips and cultured in Neurobasal medium supplemented with B27 for 24 hr. Cells were incubated with 10 μM Cy3-labeled miR-711 or miR-711(m6) in extracellular cell solution for 15 min at 37°C with 5% CO₂. Then the coverslips were washed and incubated with TRPA1 primary antibody (Alomone lab, rabbit, 1:100) at 4°C for 1 hr. The cells on coverslips were incubated with secondary antibody conjugated to FITC (1:100; Jackson ImmunoResearch, West Grove, PA) and examined under a Leica SP5 inverted confocal microscope.

RNA Pull-Down Assay and Immunoblotting

hTRPA1-expressing HEK293 cells of equal amount (~5x10⁶) were plated onto 60 mm dishes, and 24 hr later, these cells were incubated with biotin-conjugated miR-711 or miR-711(m6) in extracellular solution containing 140 mM NaCl, 5 mM KCl, 2 mM CaCl₂, 1 mM MgCl₂, 10 mM HEPES, and 10 mM glucose, adjusted to pH 7.4 for 15 min at 37°C with 5% CO₂. For crosslinking, 1% formaldehyde (vol/vol) was added at 37°C for 10 min, then 12.5% glycine was applied to stop crosslinking by 5 min incubation at room temperature. Then the cells were collected and sonicated with ultrasonic probe sonicator (80% output, 5 s on and 10 s off) in 1 mL lysis

buffer (1% Triton X-100, 50 mM Tris-HCl, 150 mM NaCl, 5 mM EDTA, pH7.4) on ice for 2 min. We then centrifuged the lysate at 13,000 rpm for 10 min at 4°C and took 50 µL supernatant as lysate control. The remaining supernatant was added 20 µL streptavidin agarose beads and incubated overnight. The pellets were collected after centrifuge at 6000 rmp for 30 s. For competing assay, miR-711 (10–50 µM) or mutant miR-711 (m6, 10–50 µM) were added 15 min before the incubation with biotin-conjugated miR-711 (10 µM). For immunoblotting, the lysates or beads were incubated in SDS-PAGE loading buffer for 30 min at 50°C, and supernatant was collected after centrifugation at 13000 rpm and decrosslink at 99°C for 20 min. The samples were separated on an SDS-PAGE gel, transferred, and probed with TRPA1 antibody (1:1000; Alomone labs). The immunoreactive bands were detected with horseradish peroxidase-conjugated secondary antibody, visualized with enhanced chemiluminescence (Thermo scientific, Pittsburgh, PA), and quantified with Image-Pro Plus software (Media Cybernetics, Bethesda, MD). Each experiment was repeated at least three times.

Fluorescent *In Situ* Hybridization (FISH)

Digoxigenin (DIG)-labeled miRCURY LNA Detection probe against hsa-miR-711 “CTTACGTCTCTCCCTGGGTC,” and negative control “GTGTAACACGTCTATACGCCCA” were used for *in situ* hybridization. After transcardiac perfusion with 4% paraformaldehyde, mouse tumor and skin tissues were dissected. FISH was carried out according to the manufacturer’s guide. Tissue sections were cut in cryostat at 14-µm thickness. The sections were fixed with 4% paraformaldehyde for 10 min at room temperature and acetylated at room temperature for 10 min. Probes were diluted with Hybridization buffer to 50 nM and hybridized at 55°C overnight. Sections were then incubated with alkaline phosphatase conjugated anti-DIG (1:3500; Roche) overnight at 4°C. After washing, the *in situ* signals were developed with Fast Red substrate. For quantification, four or five tumor sections from each mouse were selected, and three mice were analyzed in each group. To quantify the percentage of labeled cells, the number of positive cells within one field were divided by the total area of the field to obtain the density of cells. Images were analyzed with Image-Pro Plus5.1 (Media Cybernetics) or Adobe PhotoShop.

miRNA Measurement by Quantitative Real-Time RT-PCR (qPCR)

Total RNA was isolated from serum of CTCL mice or adenovirus-treated mice using Qiazol Lysis Reagent (QIAGEN) together with miRNeasy Serum/Plasma Kit (Park et al., 2014). All RNA samples were immediately used or kept at –80°C until further processing. To convert mature miRNA into cDNA, 6 µl of total RNA solution were reverse transcribed using the miScript II RT Kit (including polyadenylation of miRNAs and reverse transcription using an oligo-dT that binds to a universal RT-sequence). Specific miRNA levels were quantified by qPCR using miScript SYBR Green Kit including miScript miRNA assay for hsa-miR-711, hsa-miR21, hsa-miR155, and hsa-miR-326, together with the universal RT primer, according to the manufacturer’s protocol (CFX96 Real-Time system, Bio-Rad). Relative quantities of miRNAs were calculated using the Ct value after normalization to control miRNAs. *Caenorhabditis elegans* miRNA-39 (cel-miRNA-39) was included as spiked-in control for extracellular miRNA.

Computer Simulations

To elucidate the binding modes and interaction energies of specific miRNA sequences to TRPA1, we generated the structural model of the complex between TRPA1 and the miRNA sequence GGGACCC, which appears to be an essential for TRPA1 activation and itch induction. We generated the initial structural model of TRPA1 starting from the coordinates of the human isoform of the protein, which has been recently solved via cryo-electron microscopy at 4.24 Å resolution (pdb-id: 3j9p) (Paulsen et al., 2015). We refined the structural features of TRPA1 by introducing the missing extracellular loops using MODELER (Webb and Sali, 2014). The ion channel structure was then optimized by means of a short discrete molecular dynamics simulation (DMD) (Dokholyan et al., 1998; Shirvanyants et al., 2012), which consisted of 5×10^5 time steps at temperature 0.5 kcal/(mol k_B) corresponding to ~25 ns and ~250 K, respectively. The quality of the DMD-generated lowest energy conformation of TRPA1 was assessed using Gaia (<http://redshift.med.unc.edu/chiron/login.php>), our in-house developed software, which compares the intrinsic structural properties of our computational model to high-resolution crystal structures (Kota et al., 2011). Our modeled TRPA1 structure was well within the bounds of high-resolution crystal structure parameters in Gaia database and, thus, further adopted for computational studies in the presence of miRNA.

In a second stage, using iFoldRNA, an in-house developed methodology for RNA structure prediction with near atomic resolution accuracy (Krokhutin et al., 2015; Sharma et al., 2006), we generated the structural model of the miRNA711 core sequence GGGACCC, which was randomly positioned at a distance of 25 Å from the extracellular TRPA1 surface. In order to explore the GGGACCC sequence’s ability to bind TRPA1, we employed the replica-exchange sampling method (Zhou et al., 2001) implemented in DMD (RexDMD) (Dokholyan et al., 1998; Shirvanyants et al., 2012). In RexDMD, multiple simulations (replicas) of the same system are performed in parallel at different temperatures, and are coupled through a Monte Carlo-based algorithm for the exchange of temperatures at recurrent time intervals. This simulation scheme allows to overcome energy barriers and to efficiently explore the binding free energy surface of the GGGACCC /TRPA1 system. We used 18 parallel replicas with temperatures ranging from 0.3 to 0.6 kcal/(mol k_B) (corresponding to ~175 K and 310 K, respectively) with increments of either 0.01 or 0.02 kcal/(mol k_B). In each system the position of miRNA711ps’ center of mass was constrained within a maximum radius of 15 Å from TRPA1 extracellular surface, and every replica is simulated for 2 million time steps (i.e., ~100 ns).

With the aim of isolating the most relevant structural model of the GGGACCC /TRPA1 complex, we retrieved all configurations of the system in which the estimated interaction energy between the two species was equal or lower than –75 kcal/mol (i.e., peak of left

shoulder in the interaction energy distribution). We then clustered the retrieved high-affinity GGGACCC /TRPA1 conformational ensemble according to the root mean square deviation (RMSD) of the miRNA sequence's phosphorus atoms, using the unweighted pair group method with centroid (UPGMC) as implemented in the Python SciPy library (<https://scipy.org>). For the clustering analysis we imposed a cutoff of 4.24 Å (i.e., resolution of TRPA1 structural coordinates) to distinguish two distinct GGGACCC /TRPA1 conformations. The entries of the most populated cluster (~4% of the isolated conformational space) were analyzed to explore the binding mode of GGGACCC to TRPA1, and the lowest estimated binding energy conformation of the ensemble (i.e., -87 kcal/mol) was chosen as the representative structure of the GGGACCC/TRPA1 complex.

In order to assess the stability of the identified GGGACCC sequence's binding mode we performed five independent, 4.5×10^5 step-long DMD simulations at temperature 0.3 kcal/(mol k_B), corresponding to ~20 ns and ~175 K, respectively. We monitored the fluctuation of GGGACCC sequence's bound conformation by measuring the RMSD of its phosphorus atoms, as well as the standard deviation of the interatomic distances between GGGACCC and TRPA1 residues within 5 Å of each nucleobase. The RMSD of GGGACCC phosphorus atoms averaged around 1.75 Å. Similarly, the fluctuations of the inter-atomic distances between GGGACCC and TRPA1 were far below the resolution of the TRPA1 cryo-electron microscopy structure (Paulsen et al., 2015) (i.e., the value beyond which two atoms cannot be distinguished as different), indicating that identified binding mode is stable and consistent with the experimental structural data.

QUANTIFICATION AND STATISTICAL ANALYSIS

All data were expressed as mean \pm SEM, as indicated in the figure legends. Statistical analyses were completed with Prism GraphPad 6.0. Biochemical and behavioral data were analyzed using two-tailed Student's t test (two groups), One-Way or Two-Way ANOVA followed by post hoc Bonferroni test. Electrophysiological data were tested using one-way ANOVA (for multiple comparisons) or two-tailed Student's t test (two groups), as shown in our previous studies (Park et al., 2014; Xu et al., 2015). The criterion for statistical significance was $p < 0.05$.

DATA AND SOFTWARE AVAILABILITY

No custom software was used in this study.